RMetS
Royal Meteorological Society

Effects of the Alps and Apennines on forecasts for Po Valley convection in two HyMeX cases

Emanuela Pichelli,[a,c]* Richard Rotunno[b] and Rossella Ferretti[c]
[a]*Abdus Salam International Centre for Theoretical Physics, Earth System Physics department, Trieste, Italy*
[b]*National Center for Atmospheric Research, Boulder, CO, USA*
[c]*CETEMPS, Department of Physical and Chemical Sciences, University of L'Aquila, Italy*

*Correspondence to: E. Pichelli, ICTP (ESP), Str. Costiera, 11, 34151, Trieste, Italy. E-mail: emanuela.pichelli@aquila.infn.it; pichelli@ictp.it

Two Intensive Observation Periods (IOPs) of the Hydrological cycle in the Mediterranean eXperiment (HyMeX) are examined in this study. IOP6 and IOP13 were characterized by troughs with associated cold fronts entering the western Mediterranean and, in both cases, organized frontal convection in the Po Valley was observed. These similarities notwithstanding, predictability of the Po Valley convection was limited for IOP6 for most of the forecast models available during HyMeX, but not for IOP13. Using the Weather Research and Forecast (WRF) model in research mode, the present study confirms the relatively good forecast for frontal convection in IOP13 is not very sensitive to modelling assumptions. In contrast, it is found that only a two-way-nested simulation, initialized close to the event, was able to produce a realistic representation of the squall-line in the Po Valley for IOP6. A comparison between a 'successful' and an 'unsuccessful' simulation of the Po Valley convection in IOP6 suggests the sensitivity lies with the orographic flow modification which was at the threshold between 'flow-over' and 'flow-around' responses to the Maritime Alps. In particular, in the 'flow-over' regime, downslope winds from the Maritime Alps and Apennines suppress the convergence/uplift where the front encounters the barrier wind in the Po Valley, while in the 'flow-around' regime it is unimpeded. A delicate balance between the competing mechanisms of orographically induced subsidence on the lee side of the Apennines and frontal uplift in the Po Valley is found to be crucial for squall-line survival.

Key Words: convection predictability; complex orography meteorology; HyMeX; front blocking

Received 27 October 2016; Revised 8 June 2017; Accepted 12 June 2017; Published online in Wiley Online Library

1. Introduction

HyMeX (Hydrological cycle in the Mediterranean eXperiment; http://www.hymex.org) is a long-term project that aims at advancing the knowledge of water-cycle variability in the Mediterranean across space- and time-scales (Drobinski *et al.*, 2014). Within the envisaged 10-year activity of HyMeX, shorter observation periods are planned; the first Special Observation Period (SOP1) was dedicated to the documentation of Heavy Precipitation Events (HPEs), Flash Flood Events (FFEs) and ORographic Precipitation events (ORPs) over target areas around the western Mediterranean basin during the autumn of 2012 (5 September–5 November) (Ducrocq *et al.*, 2014; their Figure 1). This paper presents a comparative study of some critical aspects of numerical model performance for cases of convection observed in the Po Valley (Italy) during SOP1.

Previous campaigns, such as the Mesoscale Alpine Program (MAP; Bougeault *et al.*, 2001) identified many mechanisms and factors contributing to HPEs in the Alpine region. Among the factors reviewed in Rotunno and Houze (2007, p. 818) is 'Fronts passing the Alps' where the difficulty was noted in predicting the effects of eastward-moving troughs on the wind field in the wake of the western Alps, i.e. in the Po Valley, which is the geographical area considered in this study (Figure 1(a)). The Po Valley is characterized by almost level terrain surrounded by mountains on three sides: the Alps (north and west) and the Apennines (south). With the Tyrrhenian Sea to the south and the Adriatic Sea to the east, the physical geography of the area is particularly complex and strongly influences the local meteorology. A frontal passage is known to create the most favourable conditions for severe/organized convection across the area (Morgan, 1973; Buzzi and Alberoni, 1992), however complex effects of the physical geography on the mesoscale flows strongly influence the predictability of severe convection (Buzzi and Alberoni, 1992; Barrett *et al.*, 2014; Miglietta *et al.*, 2016), which remains a major issue especially in cases that turn into

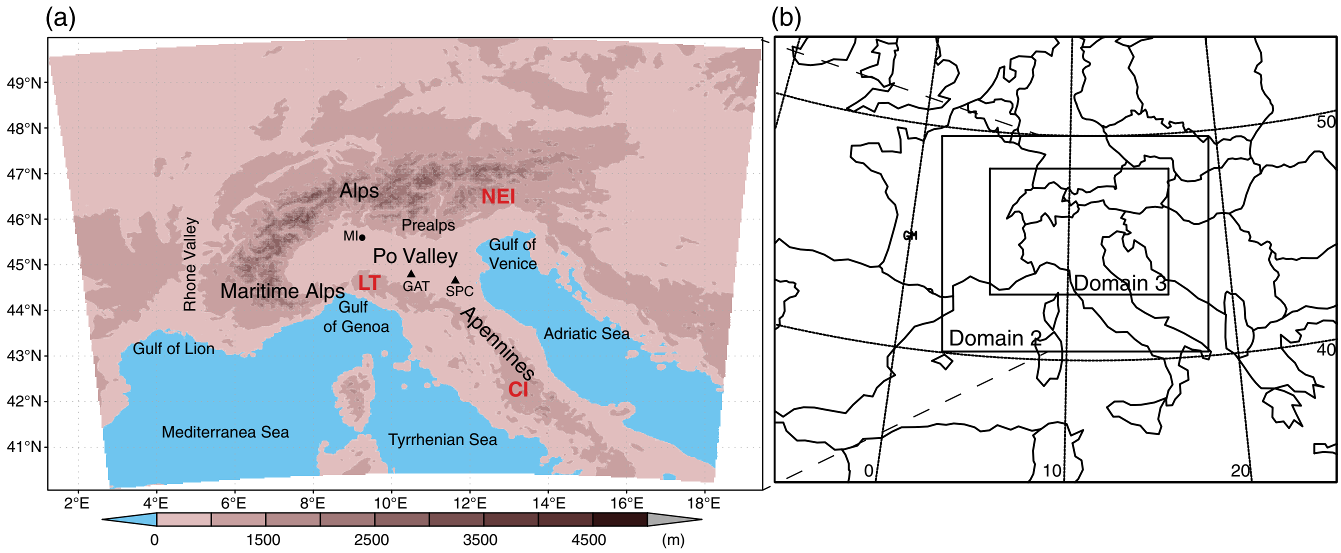

Figure 1. (a) Geography and orography of the area of interest; the triangles mark the position of the radars at Gattatico (GAT; 44.79°N, 10.49°E) and San Pietro Capofiume (SPC; 44.65°N, 11.62°E) in the Po Valley; the bullet indicates the location of the Milan radio soundings (MI; 45.43°N, 9.28°E). The three Italian target areas are indicated as LT (Liguria-Tuscany), NEI (Northeastern Italy) and CI (Central Italy). (b) Configuration of WRF Domains 1, 2, and 3 with respective resolutions of 9, 3 and 1 km. [Colour figure can be viewed at wileyonlinelibrary.com].

flood events across catchments in the Alpine area (Borga *et al.*, 2007; Panziera *et al.*, 2015).

Among the key factors influencing convection in the Alpine and surrounding areas are: lee cyclogenesis induced by the unique geomorphology of northern Italy (Morgan, 1973) which favours organized convection in the Po Valley (Cacciamani *et al.*, 1995); deformation of frontal systems crossing the Alps due to the influence of the local orography on the large-scale flow (Buzzi and Alberoni, 1992); low-level flow modifications due to the shape of the mountain barrier (Rotunno and Ferretti, 2001); moisture supply by air masses flowing over the western Mediterranean (Buzzi and Foschini, 2000; Rotunno and Houze, 2007); moisture effects on static stability influencing the air mass to flow either over or around the barrier (Buzzi *et al.*, 1998; Ferretti *et al.*, 2000; Rotunno and Houze, 2007); and cold pools in the Po Valley influencing the rainfall distribution (Rotunno and Ferretti, 2003; Reeves and Lin, 2006). Moreover, Medina and Houze (2003), provided a distinct microphysical differentiation between unstable unblocked and stable blocked cases, with the former showing embedded convection within the stratiform precipitation, inducing locally heavy rain at all levels of the Alpine slope. Experimental confirmation of these previous studies can be found in Panziera *et al.* (2015), which also highlights the potential of some meteorological quantities (such as the intensity and direction of the flow at different levels, the upstream moist static stability, etc.) as possible predictors for nowcasting applications. Recently, Davolio *et al.* (2016), also studying cases from HyMeX SOP1, presented evidence for the role of pre-existing cold air in the eastern Po Valley which acts to lift low-level conditionally unstable flow from the Adriatic and thereby trigger convection over the eastern Po Valley.

Even this short overview of the large literature on the topic illustrates the complexity of the meteorological phenomena over northern Italy. Moreover, this complexity is reflected in the difficulty in predicting convection events across the Po Valley, as confirmed by local forecasters (personal communications with collaborating forecasters from the Operational Center of L'Aquila during SOP1 and the meteorological agencies of Piemonte, Veneto, Liguria and Friuli Venezia Giulia). HyMeX cases IOP6 and IOP13 presented the opportunity to examine this difficulty in greater detail with enhanced observations and more advanced modelling capabilities.

The Italian scientific community was engaged in SOP1 with both experimental and modelling activities (Davolio *et al.*, 2015), including large deployments of advanced instrumentation (Ferretti *et al.*, 2014; their Tables 1–3). Forecasts during SOP1 were made in consultation with many different mesoscale models (Ferretti *et al.*, 2014; their Table 4) to provide guidance for events of interest over the Italian target areas, Liguria-Tuscany (LT), Northeastern Italy (NEI) and Central Italy (CI); the Po Valley extends along an east–west axis between LT and NEI (Figure 1(a)).

In several of the IOPs of SOP1, convection was both observed, and correctly forecasted, over the Po Valley; however in a few cases most of the models showed little or no skill. IOP6 was such a case and thus it was selected for this study. The convection was associated with a cold front moving from west to east across Italy. As with other models used operationally during the field campaign, the WRF model used in the present study showed an overly rapid suppression of convection in the Po Valley, just a few hours after the cold front crossed over the Maritime Alps (Figure 1(a)). In contrast, the WRF model (among others) generally forecasted convection well over the same area under similar large-scale conditions observed during IOP13. Both IOPs were characterized by troughs entering the Mediterranean basin from the west, but the two events had certain differences in their respective intensities of the large-scale forcing and mesoscale flows that proved decisive in enhancing the predictability of convective activity in the Po Valley in IOP13.

The purpose of this paper is to add knowledge to the general understanding of the physical processes and the predictability of convection in the Po Valley. Starting from the identification of similarities/differences between the two IOPs, we will then focus more on the differing roles of the local forcing of convection for IOP6. The study sheds light on the delicate balance among the mesoscale mechanisms either promoting or suppressing convection in the Po valley. In particular we found that when the flow upstream of the Alps and Apennines is at the threshold between 'flow-over' and 'flow-around' configurations, the downstream (Po Valley) evolution of convection is very sensitive to different mesoscale model forecasts. The plan of the present study is as follows: an overview of IOP13, through observations and operational forecasts available during SOP1, is

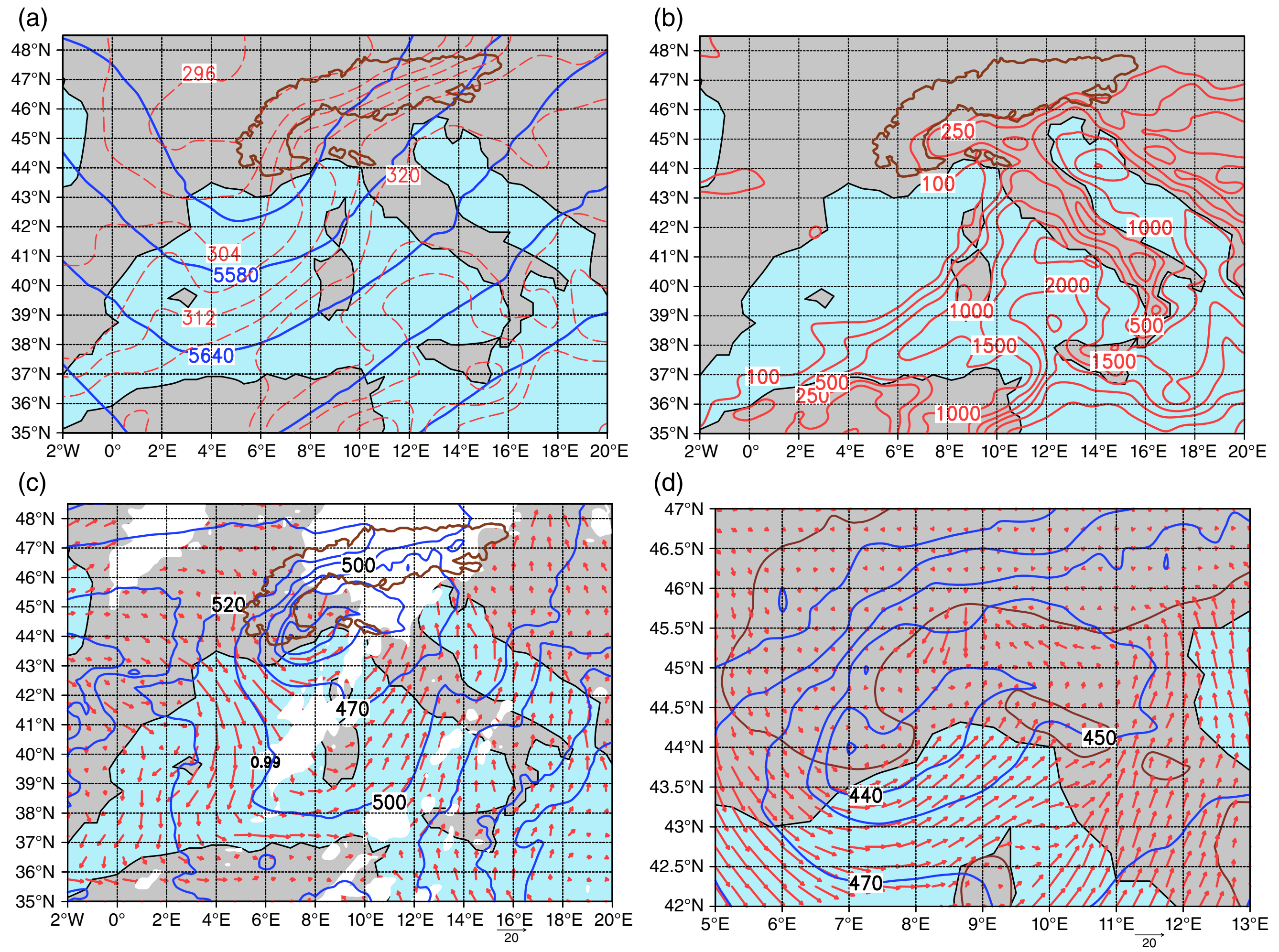

Figure 2. ECMWF analysis for IOP13, 15 October 2012, 1200 UTC: (a) Equivalent potential temperature at 950 hPa (K, dashed red line) and geopotential height at 500 hPa (m, thick solid blue lines); (b) CAPE (J kg^{-1}, solid red lines); (c) Geopotential height (m, solid blue lines) and horizontal wind vectors (m s^{-1}) at 950 hPa; 0.99 cloud-cover mask (white). (d) shows the same fields as (c), except for cloud cover, enlarged over the area of interest. The 800 m orography contour line (brown) outlines the Alps. [Colour figure can be viewed at wileyonlinelibrary.com].

given in section 2. Section 3 presents a similar overview of IOP6 and the problem encountered in the prediction of convection across the Po Valley in this case. Section 4 describes a number of model sensitivity experiments carried out in an effort to shed light on the problem encountered, along with a detailed comparison with observations. Section 5 presents a comparative analysis between the two different WRF simulations performed to better understand the problem. Conclusions are given in the final section.

2. IOP13: analysis and SOP1 model forecasts

IOP13 was declared based on forecasts of HPEs affecting the Italian target areas on 15 October 2012. The precipitation observed in IOP13 was associated with a deep, eastward-moving, upper-level trough with an associated surface cold front (Figure 2(a)). The low-level southwesterly flow associated with the trough advected warm moist and unstable air (Figures 2(a) and (b)) across Italy, contributing to an HPE and an ORP over LT and NEI.

The cold front passed over the western Alps during the night of 14 October 2012 and then moved eastward along the Po Valley where observations indicated the lower troposphere was unstably stratified; a convective system moved eastward in association with the front (the 0.99 cloud-cover mask in Figure 2(c)). By midday on 15 October 2012 the upper-level trough passed through the Gulf of Genoa and cyclogenesis occurred in the lower atmosphere, extending to most of the Po Valley (Figures 2(c) and (d)). This 'lee cyclone' contributed to the convective instability throughout the area, bringing moist air into the valley from the Gulf of Genoa and from the Adriatic, and favoured the formation of scattered cells over the central to eastern Po Valley during the late morning and afternoon of 15 October 2012. A southeasterly flow in the lower layers (below 900 hPa near 45.5°N, 10°E; Figure 2(d)) of the northern Po Valley, likely related to the barrier wind on the south side of the Alps, began on the evening of 14 October 2012, continued during the day of 15 October 2012 and is confirmed by radio-sounding observations (not shown) in Milan (MI).

This low-level barrier wind contributed to low-level convergence in the Alpine concavity, which in turn favoured heavy precipitation over the area (Schneidereit and Schär, 2000; Rotunno and Ferretti, 2001; Asencio *et al.*, 2003; Gheusi and Stein, 2003), and across the Po Valley (Davolio *et al.*, 2016), where convective cells produced local precipitation. The 950 hPa wind field (Figure 2(c)) suggests strong flow splitting around the Maritime Alps. Based on the analysis at 0600 UTC from the European Centre for Medium-range Forecasts (ECMWF), we estimate the Froude number ($Fr = U/Nh^*$), for the flow upstream (45°N,

*Given a point (x_0, y_0), the Froude number, $Fr{=}U/Nh$, is calculated with the dry Brunt–Väisälä frequency, $N(x_0, y_0, z)$, the vertical profile of the wind component perpendicular to the barrier, $U(x_0, y_0, z)$, and the local mountain height, h.

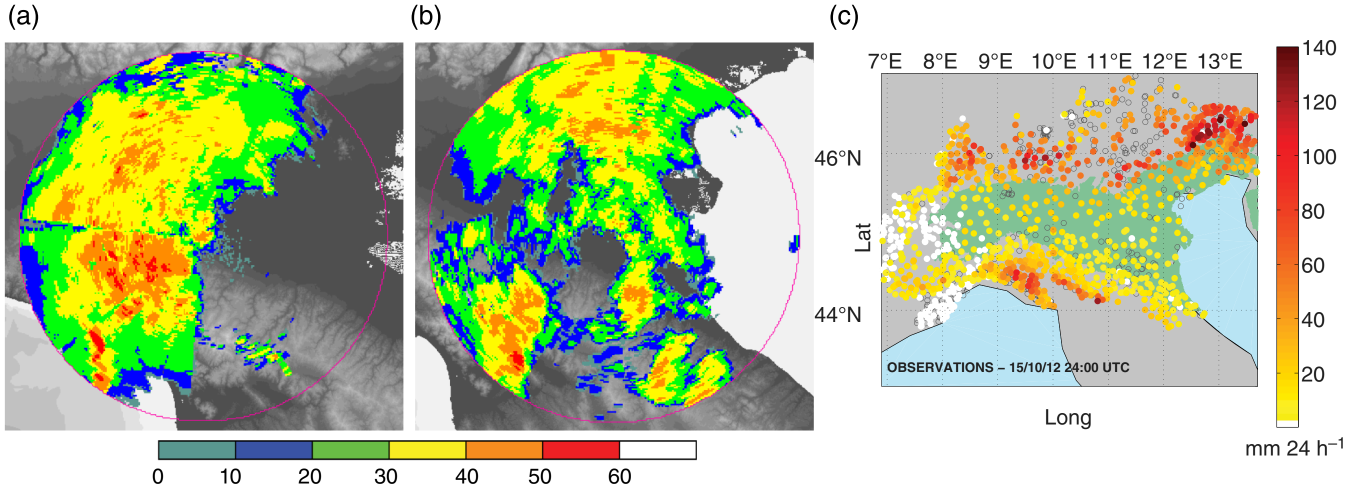

Figure 3. IOP13, 15 October 2012. Reflectivity (dBZ, colours) measured by the radar at (a) Gattatico (44.79°N, 10.49°E) at 0000 UTC), and (b) San Pietro Capofiume (44.65°N, 11.62°E) at 1200 UTC. (c) Daily accumulated rain measured by the rain-gauge network of the Italian Civil Protection department. The rain rate ranges from 3 to 140 mm $(24\,\mathrm{h})^{-1}$. The green shading shows the Po Valley. Empty circles represent stations with no valid data. [Colour figure can be viewed at wileyonlinelibrary.com].

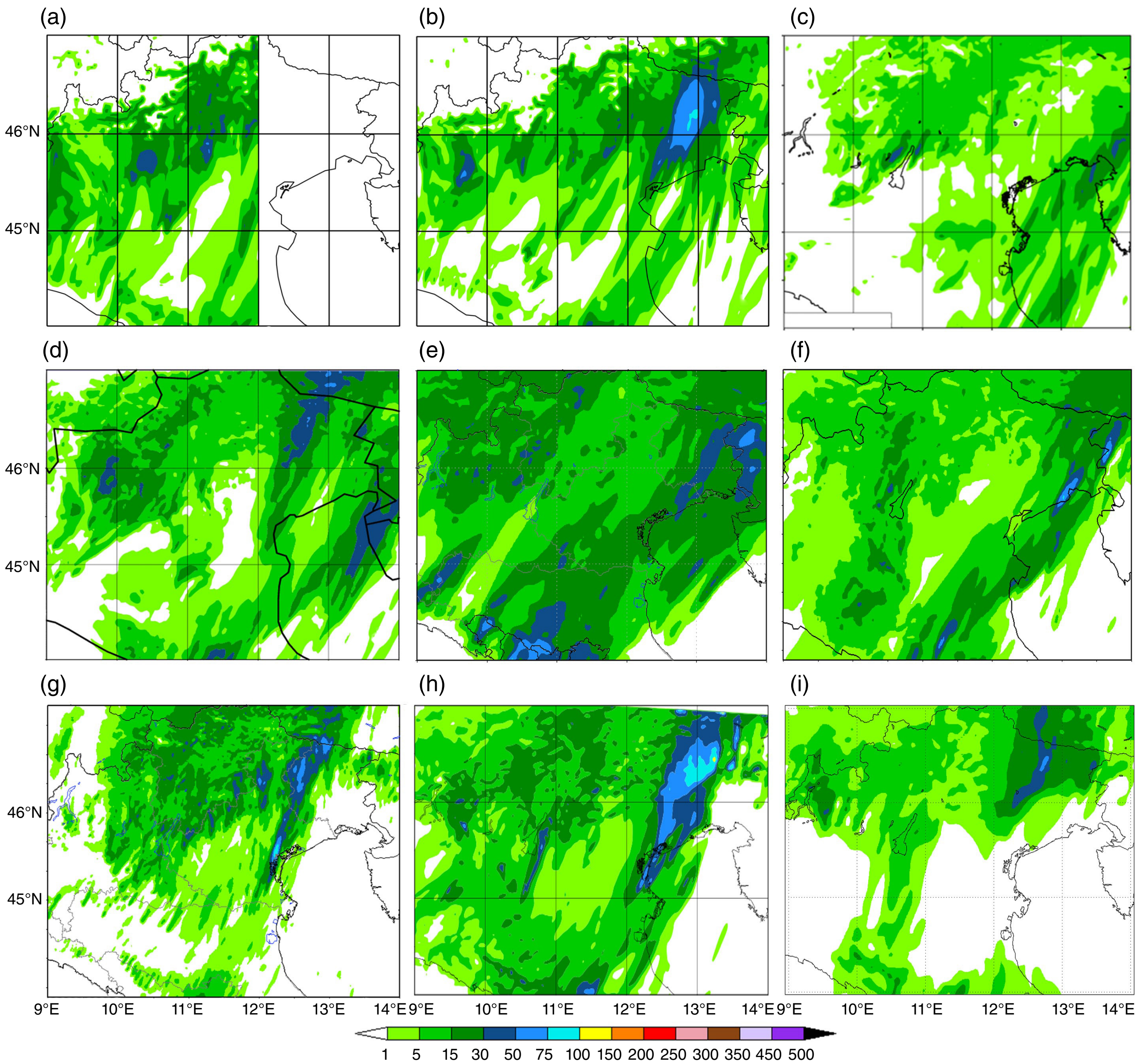

Figure 4. IOP13: forecast precipitation on 15 October 2012 over 6 h over the interval 1200–1800 UTC (but over 3 h, between 1500–1800 UTC, in (c) and (i)) by the following models available during the SOP1 of HyMeX: (a) Arome-France [1500], (b) Arome-WestMed [1500], (c) Meso-NH 2.5 km [1500], (d) Meso NH 2 km [1500], (e) WRF-LAMMA [1412], (f) WRF-ISAC [1412], (g) WRF-CETEMPS [1412], (h) Moloch-ISAC 1.5 km [1500], and (i) Moloch-ISPRA [1412]. The starting day and time is indicated as [DDHH]. Source: http://hoc.sedoo.fr. [Colour figure can be viewed at wileyonlinelibrary.com].

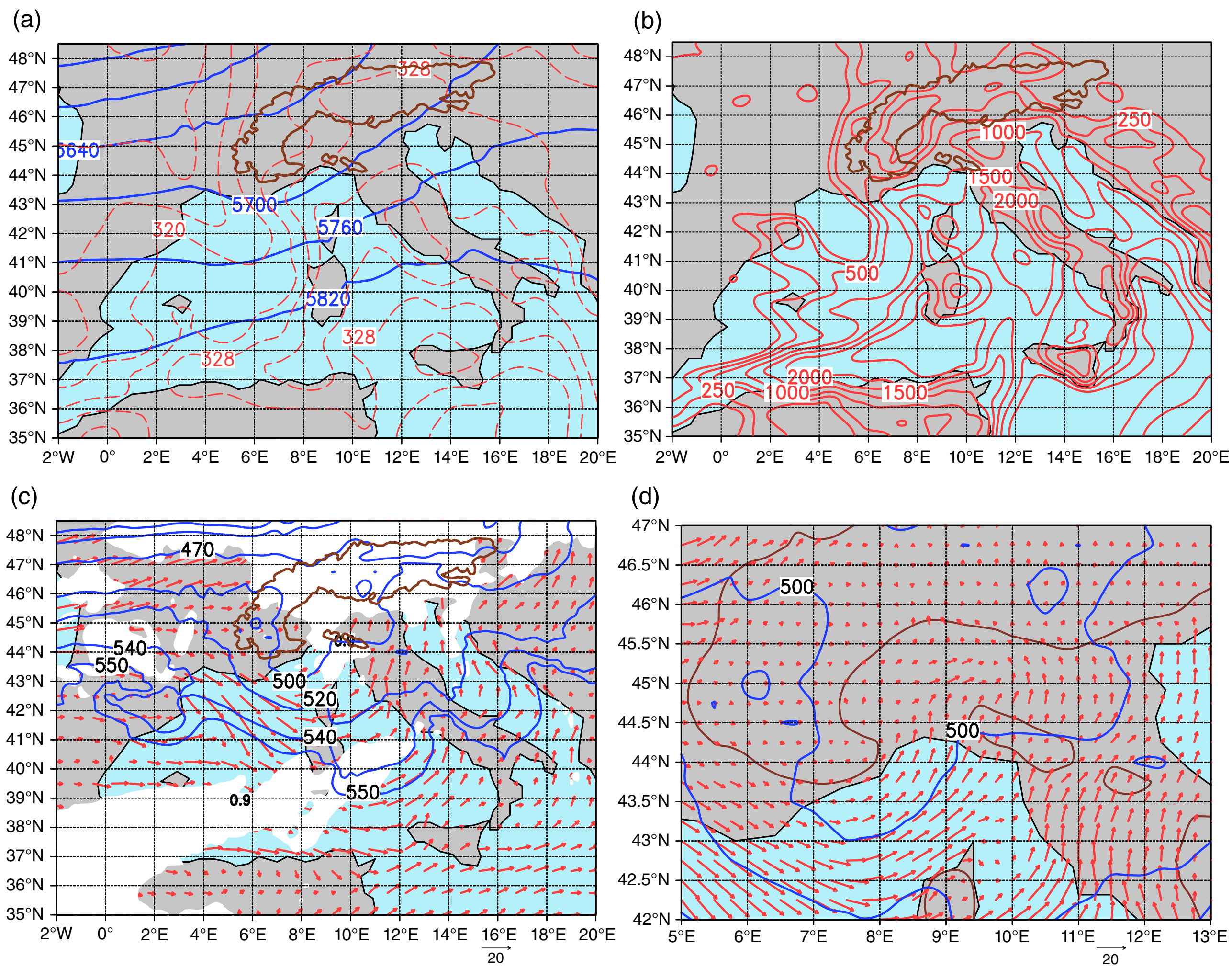

Figure 5. As Figure 2, but for IOP6 (1200 UTC on 24 September 2012) and with a cloud-cover mask of 0.9 in (c). [Colour figure can be viewed at wileyonlinelibrary.com].

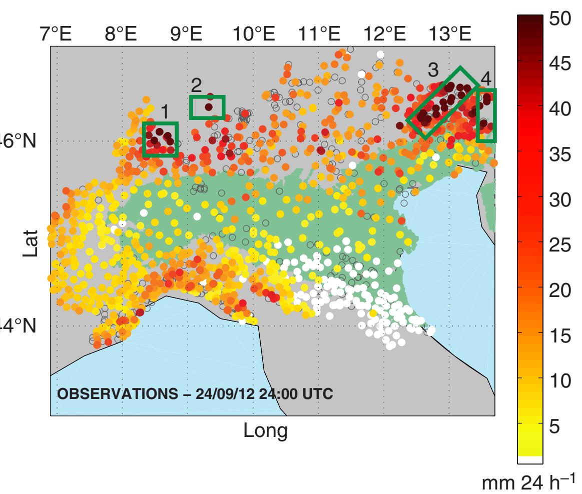

Figure 6. IOP6, 24 September 2012: daily accumulated rain measured by the rain-gauge network of the Italian Civil Protection department. The rain-rate scale is limited by 50 mm $(24\,\text{h})^{-1}$; the small rectangles highlight rain gauges that recorded larger rain rates: (1) 60–85 mm $(24\,\text{h})^{-1}$, (2) 95 mm $(24\,\text{h})^{-1}$, (3) 60–160 mm $(24\,\text{h})^{-1}$, and (4) 60 mm $(24\,\text{h})^{-1}$. The green shading denotes the Po Valley. Empty circles represents stations with no valid data. [Colour figure can be viewed at wileyonlinelibrary.com].

5.5°E) and found values in the range 0.025–0.1 below 700 hPa and in the range 0.1–0.5 between 700 and 500 hPa, thus revealing the tendency for flow blocking by the mountain barrier which forces the air to flow around it. We note that *Fr* is calculated using standard first-order finite differences in the generally unsaturated layers upstream of the mountain. Despite the limitations of the dry *Fr* applied to flows that may become saturated over mountain barriers, Barrett *et al.* (2014) argue that *Fr*, as defined here, still provides a useful characterization of the orographic flow regime.

In the late evening of 14 October 2012, the radar composites over Italy (available on http://hoc.sedoo.fr), indicated thunderstorms related to the convective squall-line that had previously developed over southeastern France, moving toward the Gulf of Genoa. By midnight, the most intense cells developed over the Gulf of Genoa (radar-estimated rain rate $\sim 50\,\text{mm}\,\text{h}^{-1}$) while weak-to-moderate ORP was detected over the LT Apennines (rain rates $\sim 15\,\text{mm}\,\text{h}^{-1}$). Organized convection was observed up to 0900 UTC (rain rates 4–8 $\text{mm}\,\text{h}^{-1}$) in the central-western Po Valley with embedded intense cells (15–20 $\text{mm}\,\text{h}^{-1}$), whereas scattered convection was recorded later towards the east.

HPEs and ORPs were observed over the Alps and Apennines by the local radars (Figures 3(a) and (b)) and by the rain-gauge network (Figure 3(c)) indicating peaks of 100–130 mm over 24 h over the central and eastern Alps along with widely scattered precipitation with values ranging between 30 and 50 mm over 24 h. The ORP over the Apennines reached maxima of between 30 and 50 mm over 24 h, with larger accumulations (100–120 mm over 24 h) associated with isolated cells. Daily accumulated rain amounts across the Po Valley range from a few millimetres to about 30 mm, with a more intense band around 10°E, where larger (40 mm over 24 h) and very localized cells were recorded.

Figure 4 shows the accumulated precipitation over 6 h (over 3 h for Moloch-ISPRA and Meso-NH 2.5 km) for the operational forecasts of some of the models available during HyMeX SOP1; different panels show different models and initializations. The

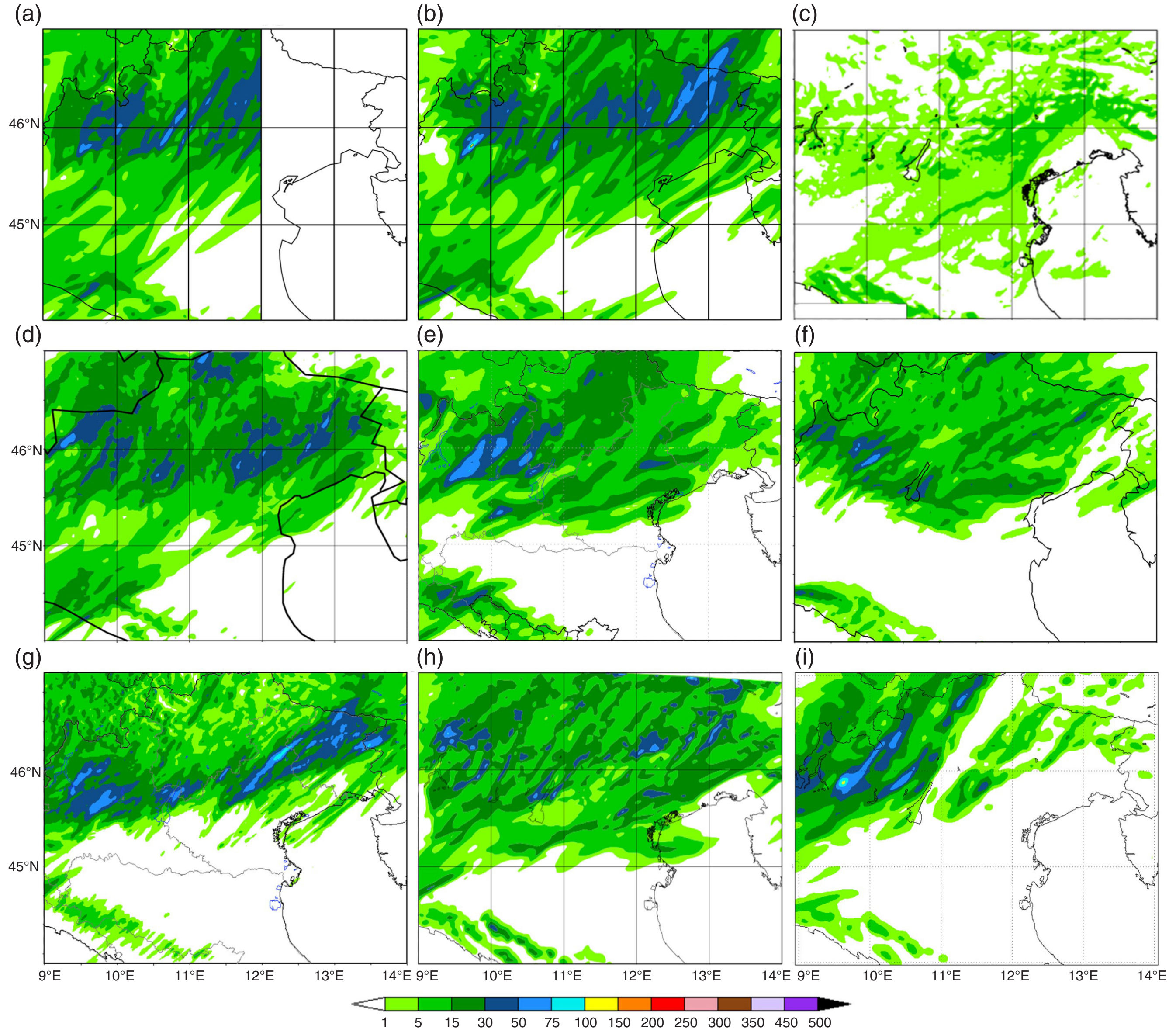

Figure 7. As Figure 4, but for IOP6. Precipitation forecast on 24 September 2012 over 6 h over the interval 1200–1800 UTC (but over 3 h between 1200 and 1500 UTC, for (c) and (i)) by the following models: (a) Arome-France [2400], (b) Arome-WestMed [2400], (c) Meso NH 2.5 km [2400], (d) Meso NH 2 km [2400], (e) WRF-LAMMA [2400]), (f) WRF-ISAC [2400], (g) WRF-CETEMPS [2312], (h) Moloch-ISAC 1.5 km [2400], and (i) Moloch-ISPRA [2312]. [Colour figure can be viewed at wileyonlinelibrary.com].

Table 1. Comparisons between IOP13 and IOP6.

Features	IOP13	IOP6
Minimum MSL	1000 hPa	1005 hPa
Lee cyclone	Yes (Figures 2(c) and (d))	No (Figures 5(c) and (d))
Upper-level trough	Deep (Figure 2(a))	Shallow (Figure 5(a))
PVA (300 hPa)	3	2
Southwesterly wind at 950 hPa	10 m s^{-1}	15 m s^{-1}
Zonal wind at 300 hPa	10 m s^{-1}	30 m s^{-1}
Maritime Alps Froude number	0.025–0.1 ($p > 700$ hPa)	0.1–0.3 ($p > 700$ hPa)
	0.1 –0.5 ($700 > p > 500$ hPa)	0.3–0.8 ($700 > p > 500$ hPa)

Minimum MSL = the mean sea level pressure minimum over northern Italy; PVA = Positive Vorticity Advection (in units of 10^{-9} s^{-2}). Source: ECMWF analyses map on http://www.eumetrain.org

interval shown, i.e. 1200–1800 UTC, represents the last phase of the event across the Po Valley. All the models, regardless of the start time, maintained convection during the entire period it was observed. The same conclusion holds true for forecasts initialized earlier. The models correctly associated the convection with both the frontal passage during the first period of the event and then with the later lee-cyclogenesis phase in the afternoon, correctly predicting rain up to 10–15mm (6 h)$^{-1}$ in the eastern part of the Po Valley (Figure 4). The second phase appears to be an example of flow entering NEI from the Adriatic; the flow was blocked by the Alps producing a barrier wind along which convection was produced in the Po Valley (Davolio *et al.*, 2016; their Figure 13a). The ten independent members of the Consortium for Small-Scale Modelling Ensemble Prediction System (COSMO-EPS; available at http://hoc.sedoo.fr) available during HyMeX (Ferretti *et al.*, 2014) also estimated surface precipitation probability between

Table 2. Summary of the experiments performed with the WRF model for the IOP6 case.

Expt.	Description	Objective	Squall-line representation across the Po Valley in IOP6
1	Nest-down (one-way) configuration: 12 km-Europe, 3 km-Italy (start time 23 Sep 2012 at 1200 UTC)	Operational forecasts during SOP1	Suppression after 1200 UTC
2	Three one-way nested domains: 12 km–3 km–1 km as in Figure 1(b) (start time 23 Sep 2012 at 1200 UTC)	Enhance the resolution over northern Italy and better represent the upstream flow over western Mediterranean with an extended domain	No beneficial effects from domain configuration and resolution changes
3	Sensitivity to PBL scheme (MYNN-CNTR, YSU, MYJ, ACM2, ACM1, BouLac)	To see whether some schemes are able to reproduce better conditions for the squall-line	The problem is common to all PBLs
4	Decrease the horizontal eddy viscosity through the constant factor C_s in the Smagorinsky formulation	Reduce the vertical flux of horizontal momentum	No improvement
5	Increase the roughness	Reduce the horizontal wind overestimation	No improvement
6	As Expt. 2, but start time 24 Sep 2012 at 0000 UTC	Use updated ICs and BCs, closer to the squall-line formation time	No improvement
7	Three one-way nested domains: 9 km–3 km–1 km as in Figure 1(b) (start time 23 Sep 2012 at 1200 UTC)	Increase the mother domain resolution to better resolve large-scale forcings	No improvement (only changes in the Alpine orographic precipitation)
8	As Expt. 7, but using three two-way nested domains	Improve the forecast through the mesoscale feedback to the low resolution	Improvements in the mid-western part of the Po Valley, but the suppression problem still persists in the mid-eastern part (present results). The horizontal wind over-estimation is reduced only at lower levels
9	Increase the number of vertical levels (from 37 to 50)	Improve the vertical column representation	No improvement
10	Increase the top level height (up to 10 hPa)	Control eventual reflections from the upper boundary	No improvement
11	As Expt. 7, but start time 24 Sep 2012 at 0000 UTC	Use updated ICs and BCs with the improved two-way simulation	The model reproduces a realistic evolution of the Po Valley squall-line

In the second column, unless indicated, the domain configuration is the same as the previous one.

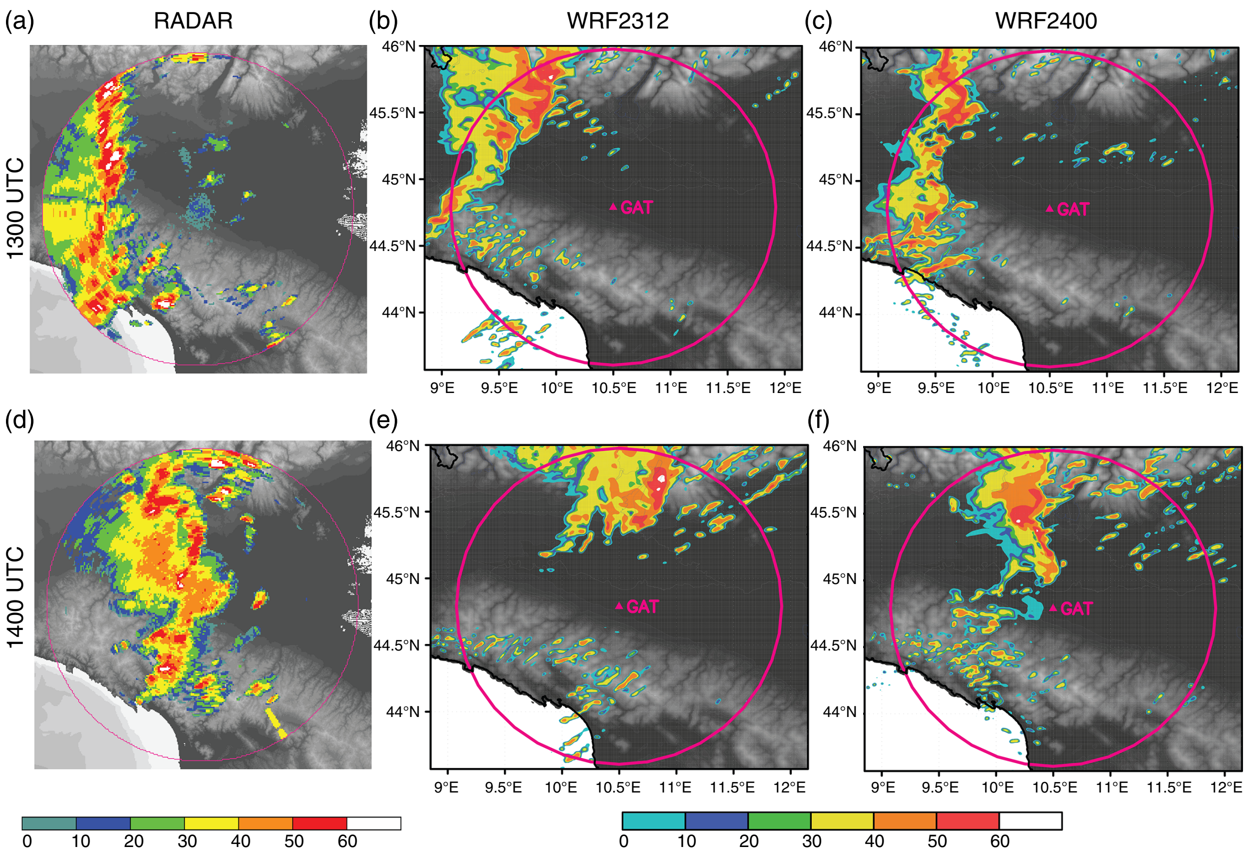

Figure 8. IOP6: reflectivity (dBZ, colours) at (a)–(c) 1300 UTC and (d)–(f) 1400 UTC on 24 September 2012. (a, d) measured by the radar at Gattatico (GAT; 44.79°N, 10.49°E, and simulated on the finest horizontal grid (1 km) at 900 hPa by (b, e) WRF2312 and (c, f) WRF2400. The background grey shading represents the orography of the area. [Colour figure can be viewed at wileyonlinelibrary.com].

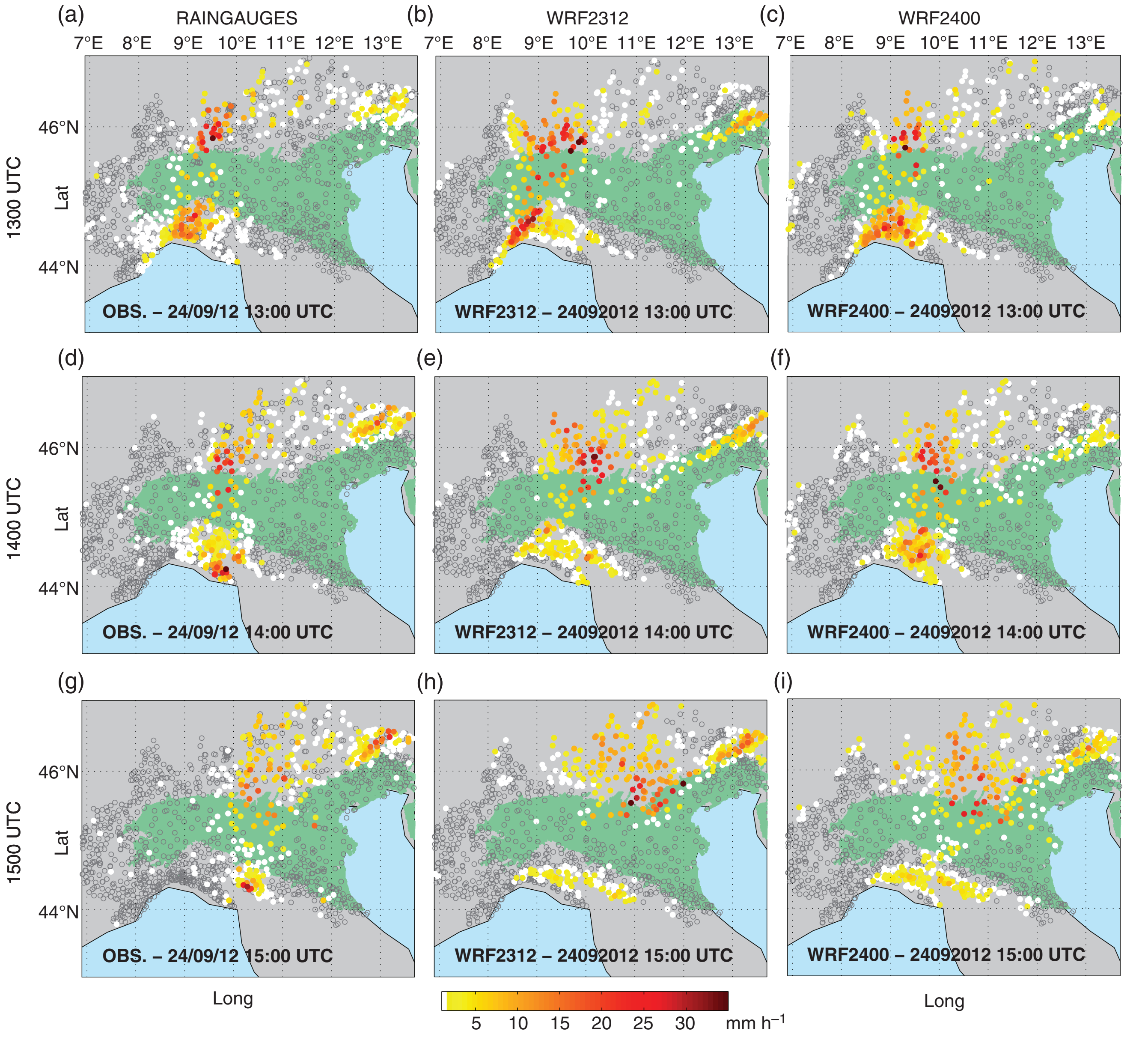

Figure 9. IOP6: one-hour accumulated precipitation (mm h^{-1}, colours) on 24 September 2012 as (a, d, g) measured by the rain gauges of the Italian Civil Protection network and as simulated on the finest horizontal grid (1 km) by (b, e, h) WRF2312 and (c, f, i) WRF2400, at (a)–(c) 1300, (d)–(f) 1400 and (g)–(i) 1500 UTC . The scale ranges between 0.2 and 35 mm h^{-1}. Empty circles represent all stations below the 0.2 mm h^{-1} threshold. The green shading shows the Po Valley. [Colour figure can be viewed at wileyonlinelibrary.com].

60 and 100% for accumulated rain exceeding 2 mm in 24 h across the Po Valley (in the area 44.7–45.5°N, 8–12°E) and for accumulated rain exceeding 10 mm in 24 h in the western Po Valley. A probability of up to 50% was calculated for accumulated rain exceeding 10 mm in 24 h in the eastern Po Valley (11–12.5°E); finally a low but non-zero probability (1–30%) was found for intense cells in the area affected by the squall-line (> 50 mm over 24 h). Based on the skill of these diverse models, a correct forecast of the convective thunderstorms across the Po Valley for this event was achieved by forecasters up to 36–48 h in advance, during SOP1 of HyMeX.

It is worth noting that most of the models shown in Figure 4 were run in a one-way operational configuration during SOP1, suggesting that the relatively good prediction in the Po Valley for IOP13 was mainly related to the large-scale forcing, which was intense enough to allow a good mesoscale prediction for a range of inner-domain resolutions (1.5 up to 3 km). Although the different models show a certain sensitivity of rain amounts and spatial distribution across the Po Valley to both initial conditions and resolution, they all produced forecasts of convective activity related to the frontal passage.

3. IOP6: analysis and SOP1 models forecast

IOP6 took place on 24 September 2012. Also in this case a North Atlantic upper-level trough moved eastward (Figure 5(a)). The interaction between the associated westerly winds over southwest Europe with the Alps produced a mesoscale lee trough associated with a surface cold front (Figure 5(b)), which moved eastward through northern Italy.

Close examination of the flow shown in Figure 5(c) suggests the flow past the Maritime Alps was not as strongly split as it was in IOP13 (cf. Figure 2(c)). The *Fr* estimated from ECMWF data upstream of the western Alps (45°N, 5.5°E) at 1200 UTC, in this case is between 0.1 and 0.3 below 700 hPa and between 0.3 and 0.8 up to 500 hPa, suggesting a lesser tendency for flow blocking by the western Alps than in IOP13 and thus a greater tendency for the air mass at the lower levels to flow over the orographic barrier rather than around it. Satellite infrared images (not shown) indicate that the front was upstream of the Alps during the night of 23 September 2012, then crossed the mountain barrier in the early morning of 24 September, gradually shifting southeastward. The frontal passage induced strong convective activity with associated

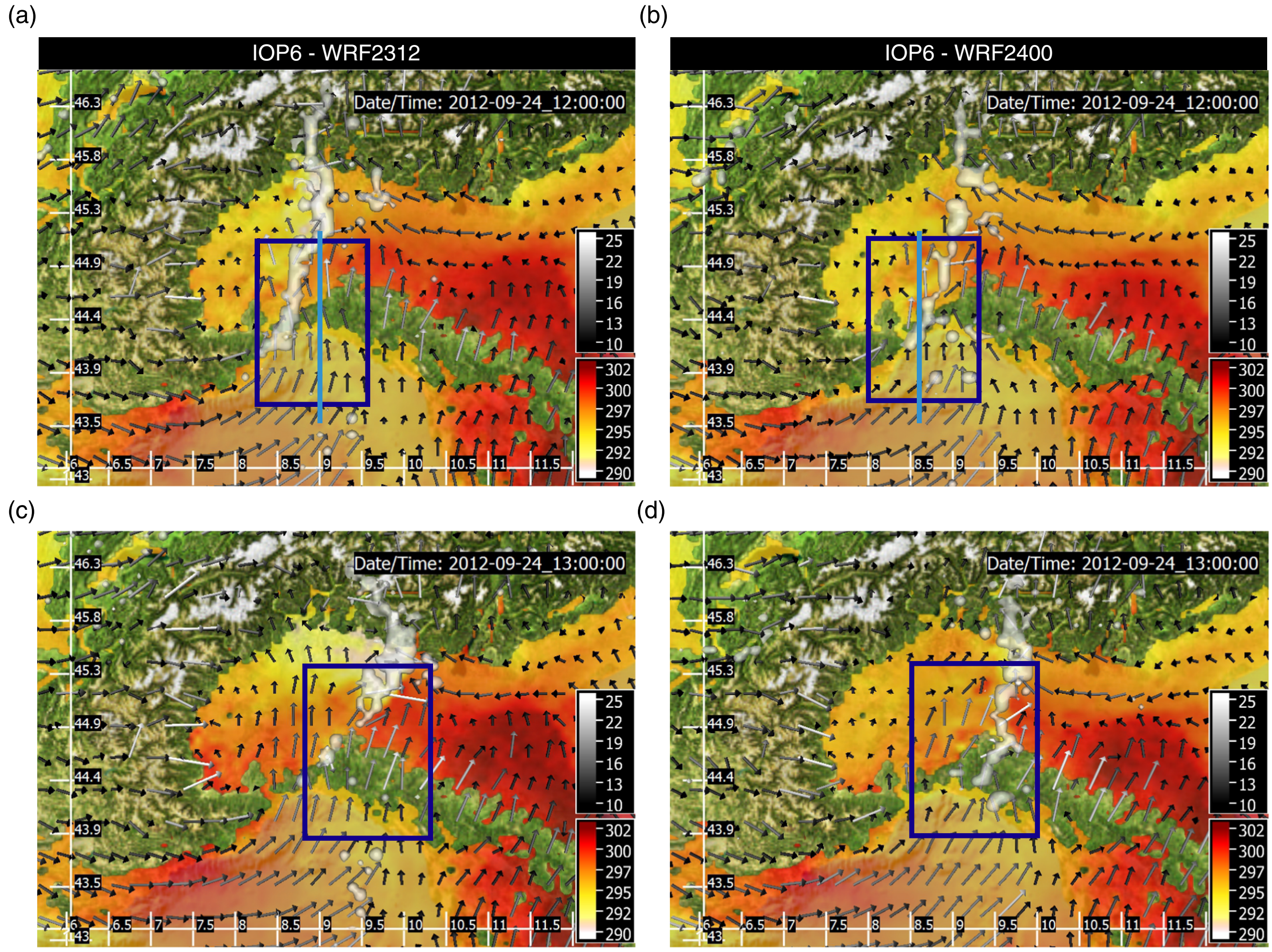

Figure 10. IOP6: horizontal wind at 200 m above the surface (barbs with grey scale, in m s^{-1}), potential temperature at 500 m (red/yellow scale in K) and 0.5 g kg^{-1} rainwater mixing ratio (white) simulated on the finest horizontal grid (1 km) by (a, c) WRF2312 and (b, d) WRF2400 at (a, b) 1200 UTC and (c, d) 1300 UTC on 24 September 24 2012. The north–south blue line in (a, b) indicates the position of the vertical cross-sections in Figure 12. [Colour figure can be viewed at wileyonlinelibrary.com].

HPEs and ORPs over the target areas of LT and NEI. An intense convective line moved from northwest to northeast Italy, crossing LT by midday (the 0.9 cloud-cover mask in Figure 5(c)), the central-eastern Po Valley between late morning/afternoon and finally NEI in the evening.

After the front passed the Maritime Alps (around 0600 UTC), the analysis in Figure 5(d) indicates a weak low-level wind from the southsoutheast at the southern edge of the Alps (45.5°N, 9.5–12.0°E), which was also confirmed by the radio soundings from Milan (not shown); in the mid-to-high troposphere (800–150 hPa) winds were from the westsouthwest during most the event. The presence of a weak easterly component of the flow on the south side of the Alps reveals a weak tendency for lee cyclogenesis, which is another feature of weak blocking upstream of the Alps (Morgan, 1973).

HPEs were observed by the rain-gauge network over the eastern Alps with a maximum of 160 mm $(24\,h)^{-1}$ (rectangle 4 in Figure 6); ORPs over both the Alps and across the LT Apennines occurred with maxima of approximately 40–50 mm over 24 h. Rain from a few millimetres to 30 mm over 24 h over the Po valley was also observed (Figure 6). Radar images (discussed below, Figures 8(a) and (d)) showed a north–south oriented convective squall-line moving eastward from the Maritime Alps across the Po Valley, with an intense cell (100 mm h^{-1}) developing over the Gulf of Genoa. The radar-derived precipitation showed cells reaching maximum rain rates of 50–70 mm h^{-1} over the western Po Valley. Later the most intense cells were observed over the northeastern Po Valley with maxima of approximately 70 mm h^{-1} and, finally, the convective front moved towards the northeastern pre-Alps and Alps.

Figure 7 shows the accumulated precipitation over 6 h (over 3 h for Moloch-ISPRA and Meso-NH 2.5 km) for model forecasts available during SOP1 in the interval 1200–1800 UTC; most of them show weak or no rain extending northwest–southeast across the eastern Po Valley. Only a few models, even when initialized at 0000 UTC on 24 September 2012, show a weak rain pattern ascribable to an organized squall-line passage up to 11°E (Figures 7(a)–(d)). Most of the models suppress the squall-line across the central-southern part of the Po Valley (Figures 7(e)–(i)). Furthermore, five of the ten independent members of the COSMO-EPS do not show any convection in the central Po Valley and none of them shows any signal of precipitation on its east side. In this case, zero probability of surface daily precipitation was found for rain above 10 and 50 mm over 24 h in the central Po Valley (44.5–45.5°N, 10–12.5°E), but a probability of 1–60% for rain above 2 mm over 24 h in the central-western part of the Po valley.

The difficulty experienced by most of the models in forecasting convection over the Po Valley in this case indicates that either the convection was inherently less predictable or that almost all the models had biases leading to an incorrect suppression of convection in the Po Valley. Table 1 contains a comparison of the most important similarities and differences between the two IOPs. One may expect the stronger large-scale forcing in IOP13 to produce

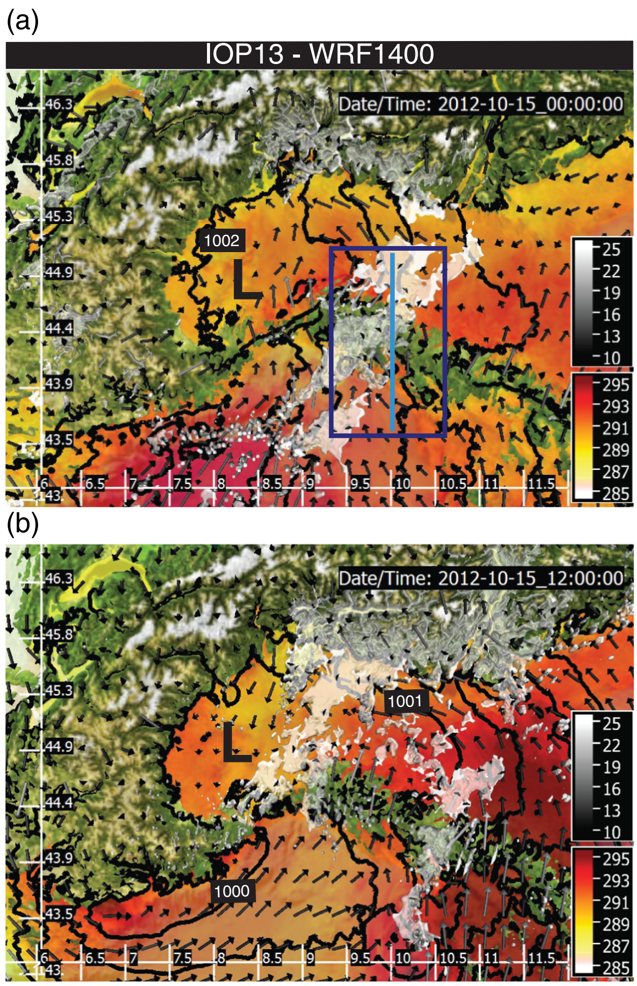

Figure 11. As Figure 10, but for IOP13 and with 0.1 g kg^{-1} rainwater mixing ratio (white) and sea level pressure (hPa, black contours at 1 hPa intervals) simulated on the finest horizontal grid (1 km) by WRF1400 at (a) 0000 UTC and (b) 1200 UTC on 15 October 2012. [Colour figure can be viewed at wileyonlinelibrary.com].

a larger signal-to-noise ratio and therefore a better chance for the models to obtain the correct forecast. By the same reasoning, the weaker large-scale forcing in IOP6 would mean a lower probability of the model producing the correct forecast. However convection is fundamentally a small-scale phenomenon and the physical connections to the larger-scale flow that made the forecast for IOP6 more difficult can only be uncovered through further study. The remainder of this paper is focused on this question.

4. Numerical simulations

The IOP6 forecast is analyzed here using the Advanced Weather Research and Forecasting (WRF) model which is a non-hydrostatic model with terrain-following vertical coordinates and multiple-nesting capabilities (Skamarock *et al.*, 2008). Three two-way-nested domains are used here in research mode (Figure 1(b)) with the innermost surrounding the Alps. The outermost domain is centred at 44.5°N, 11.5°E and has a spatial resolution of 9 km, whereas the inner-domain resolutions are, respectively, 3 and 1 km (Figure 1(b)). This configuration is not the same as used operationally by WRF-CETEMPS during SOP1 which had two one-way nested domains (12 km extended over southern Europe and 3 km over Italy). As discussed above, the incorrect inhibition of convection in the Po Valley in IOP6 was first noticed in these operational forecasts (e.g. Figure 7).

Based on a series of previous experiments (Table 2 discussed below) aimed to investigate the role of different factors on the frontal convection forecast (such as the horizontal resolution, the role of the PBL and land-surface schemes, the impact of initial conditions), the present model configuration was adopted to enhance the resolution in the Alpine region to see if the coarser resolution in the operational model and the lack of feedback from higher- to lower-resolution domains could have played a role in the model's mistaken suppression of convection in IOP6. The model is here configured as follows:

- *Vertical levels:* 37 unequally spaced vertical levels, from the surface to 100 hPa, with higher resolution in the planetary boundary layer;
- *Radiation:* Rapid Radiative Transfer Model (RRTM; Mlawer *et al.*, 1997) for long-wave, and Goddard scheme (Chou and Suarez, 1999) for short-wave radiative processes;
- *Cumulus:* Grell-3 (Grell and Devenyi, 2002) in Domain 1; none in Domains 2–3;
- *Microphysics:* Thompson *et al.* (2008) single-moment bulk scheme;
- *Boundary layer and turbulence:* Turbulent kinetic energy (TKE) scheme of Mellor–Yamada–Nakanishi–Niino (MYNN, level 2.5; Nakanishi and Niino, 2006);
- *Surface:* Monin–Obukhov–Janjić surface scheme with the Noah land-surface scheme (Niu *et al.*, 2011);
- *Damping of instabilities produced by steep topography:* Following Dudhia (1995), the 'epssm' parameter (i.e. the β coefficient in the acoustic time-step first introduced by Durran and Klemp, 1983) was set to 0.2 for the 3 km domain and to 0.4 for the 1 km domain.

The ECMWF analyses (0.125° resolution) are used for initial conditions. The boundary conditions are updated every 6 h with the ECMWF forecasts to replicate an operational-like configuration for the coarse domain; however the fine-grid boundary conditions are interpolated from the coarse-grid forecast and are passed down every coarse-domain time step.

Table 2 summarizes the experiments we performed to isolate possible causes of the incorrect suppression of convection in the Po Valley in IOP6 and to identify the configuration that best simulated the event. Expt. 1[†] refers to the model in its SOP1 forecast mode. Expt. 2 refers to the upgraded domains/resolutions depicted in Figure 1(b). Within the context of Expt. 2, the effects of different boundary-layer parametrizations were tested in Expt. 3 and, using the MYNN scheme, the Smagorinsky constant was varied (Expt. 4); Expt. 5 varied the surface roughness. None of these variations in the physics produced any relevant improvement in the experimental outcome. Further tests varying the simulation start time (Expt. 6) and Domain-1 resolution (Expt. 7) showed very little variation in the results. All the foregoing experiments (Expts. 1–7) were carried out in the forecast model using one-way nesting. The only significant improvements were obtained in the experiments with interactive inner grids (Expts. 8–11) with no improvements introduced by changes in the vertical resolution (Expt. 9) or vertical domain size (Expt. 10). The best simulation (Expt. 11) was the one initialized closest in time to the event.

A comparison between the observations and the two best WRF simulations (Expts. 8 and 11) is presented in the next subsection. The two simulations start respectively at 1200 UTC

[†]The nest-down procedure is an alternative one-way procedure that consists of running the coarse- and fine-grid domains independently. In this case boundary conditions for the fine-grid domain are still produced from the coarse-grid domain, but are passed down with a prescribed frequency, which in this case is every 2 h.

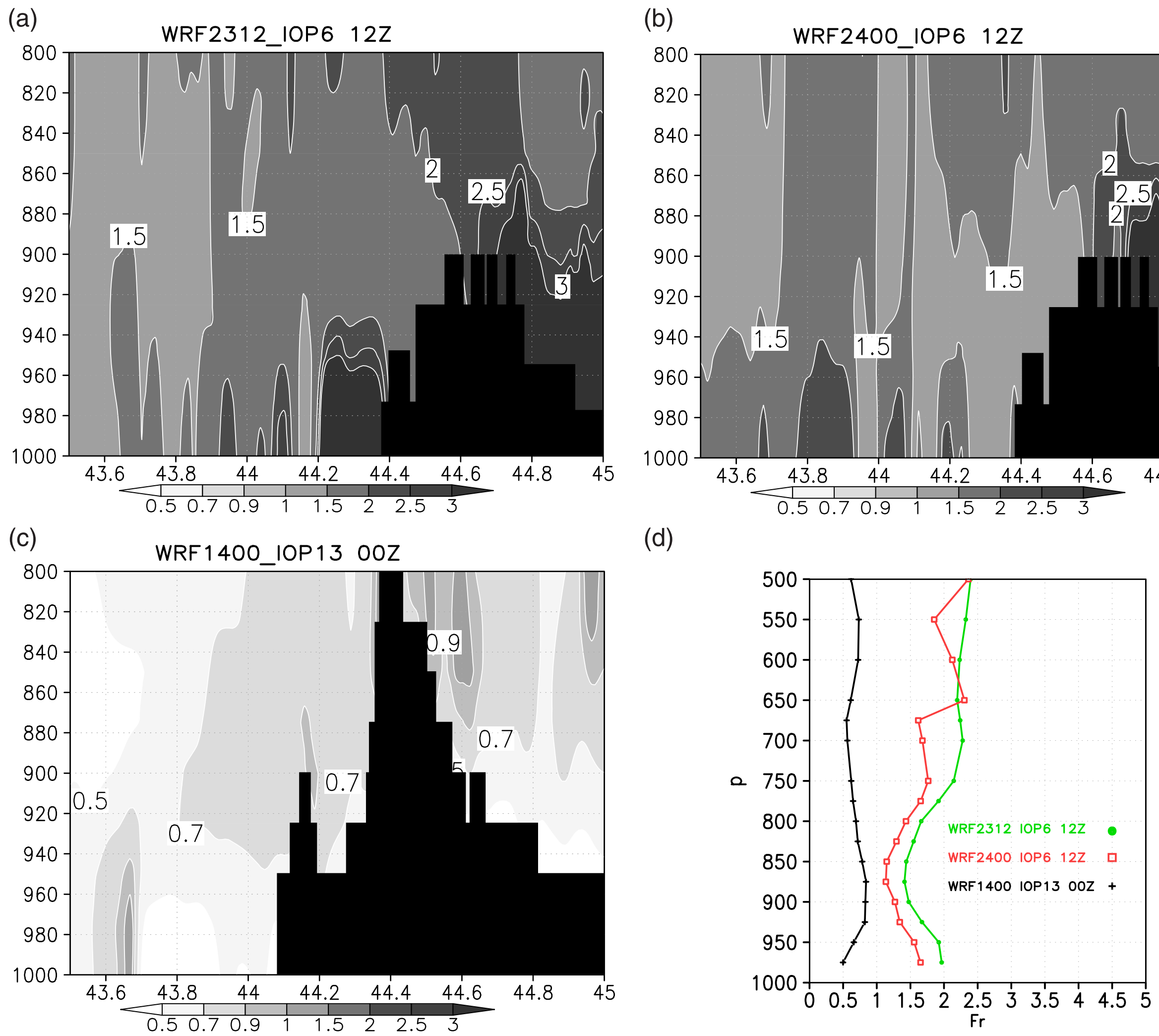

Figure 12. Vertical cross-section of the Froude number at 9°E, 43.5–45°N for IOP6 simulated by (a) WRF2312 and (b) WRF2400, and (c) at 10°E, 43.5–45°N for IOP13 simulated by WRF1400. (d) shows vertical profiles of *Fr* at the same longitudes and latitude 44°N for the three simulations (1 km domain). [Colour figure can be viewed at wileyonlinelibrary.com].

on 23 September (WRF2312) and at 0000 UTC on 24 September 2012 (WRF2400) and cover the whole duration of the IOP6. WRF2400 produces a good simulation of the squall-line across the Po Valley and thus is used as a standard of comparison for the less-successful WRF2312 with the aim of isolating the mechanisms that led to the limited predictability of the convection in the Po Valley in IOP6.

It is worth noting that in a preliminary phase of this study we performed verification tests to compare the SOP1 operational model with the available observations. Unfortunately none of the special HyMeX observations were made in the area of interest (the Po Valley specifically), but ordinary ones (ground stations, radio-soundings) were used to assess WRF wind biases. Some special observations (boundary-layer balloons) in the western Mediterranean were used for verification, however these were not useful for verification of the flow upstream of the Apennines. Except for the wind, which is generally overestimated close to the surface, no significant bias was found, especially in terms of water vapour content. This latter finding provided a solid basis on which to assess the simulations performed in Table 2. The WRF tendency to overestimate the surface wind, also found for IOP13 (which, in contrast, did not exhibit predictability problems for the precipitation across the Po Valley), is documented in the literature (e.g. Pichelli *et al.*, 2014, and references therein); the final model configuration, and in particular the choice of a local scheme for the PBL, also aims at minimizing this bias.

4.1. *WRF compared with observations*

The evolution of the convection associated with the frontal passage is shown in Figures 8(a) and (d). In the interval 1300–1400 UTC on September 24, the radar detected a squall-line with intense embedded cells (reflectivity between 50 and 70 dBZ), indicating the presence of heavy thunderstorms across the Po Valley. After 1400 UTC, cell intensity over the central-southern Po Valley was reduced (40–50 dBZ), but heavy-precipitation cells were still detected in the central-northern Po Valley and an organized line of cells reflecting frontal passage was still detectable.

The corresponding results[‡] from the innermost domain of the model simulations are shown in Figures 8(b), (c), (e), (f). Figures 8(a)–(c) show that both WRF2312 and WRF2400 reproduce the squall-line in its first phase over northern Italy (1300 UTC); however there are notable differences between the two simulations. In WRF2312 (Figure 8(b)), the squall-line axis has a northeast–southwest orientation and cells to the north of the Apennines are less intense than observed (cf.

[‡]The radar maps are built from observations at different heights depending on target distance and beam blocking. Given this analysis method and considering that the squall-line evolves across complex orography, we used an intermediate height (generally at 900 hPa) between the minimum and maximum radar height for the comparative analysis of model reflectivity. The model reflectivity is calculated using an algorithm that makes assumptions consistent with a bulk mixed-phase microphysical scheme, with constant density spherical particles following an exponential distribution as a function of their actual diameter.

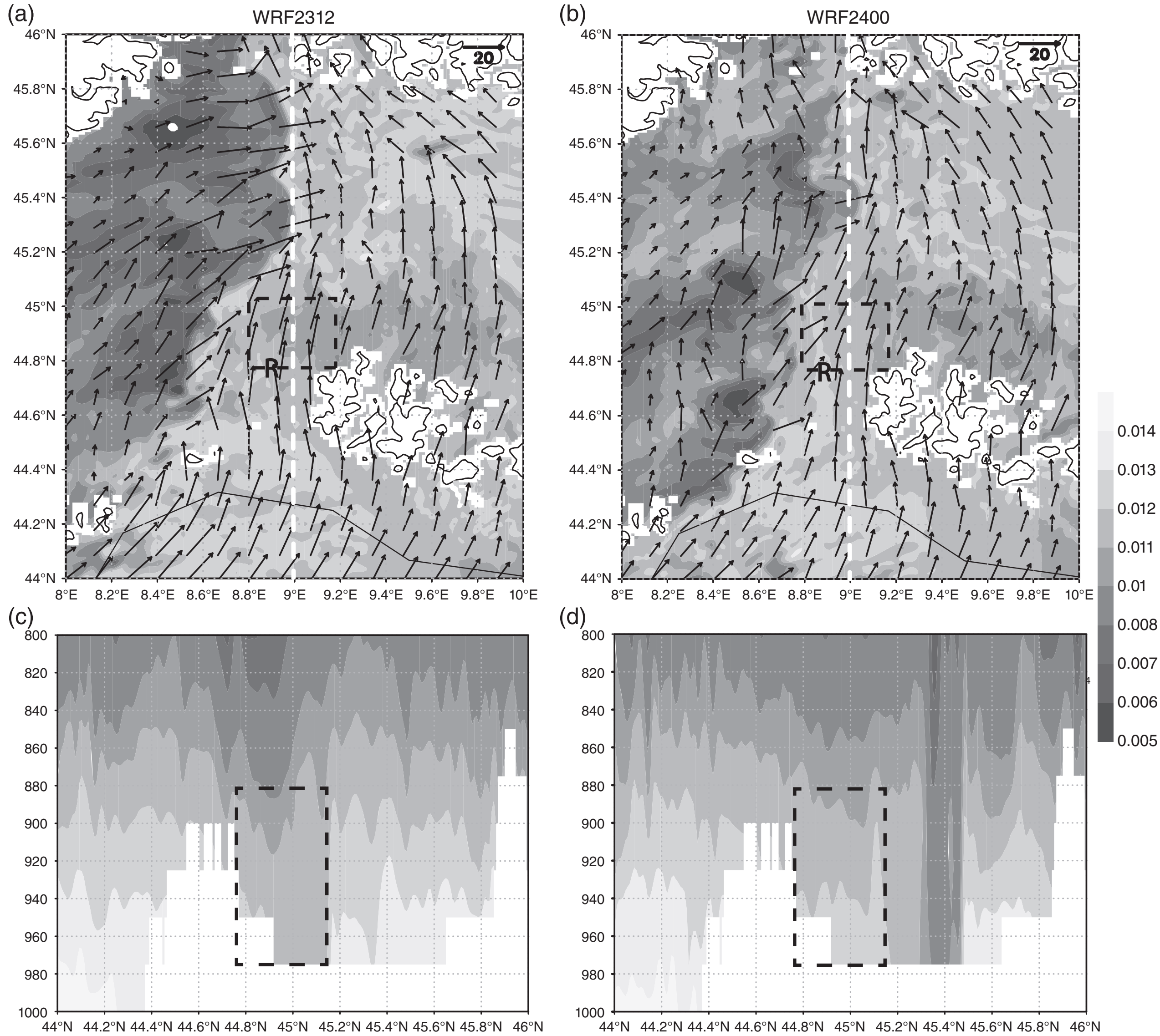

Figure 13. IOP6: water vapour mixing ratio (kg kg^{-1}, grey shading) with (a, b) horizontal wind vectors at 900 hPa and (c, d) vertical cross-section at 9°E, 44–46°N (along white dashed line in (a, b)) simulated on the finest horizontal grid (1 km) by (a, c) WRF2312 and (b, d) WRF2400 at 1200 UTC on 24 September 2012. The black-dashed boxes indicate the areas to be compared between WRF2312 and WRF2400 to highlight the drying subsidence in WRF2312.

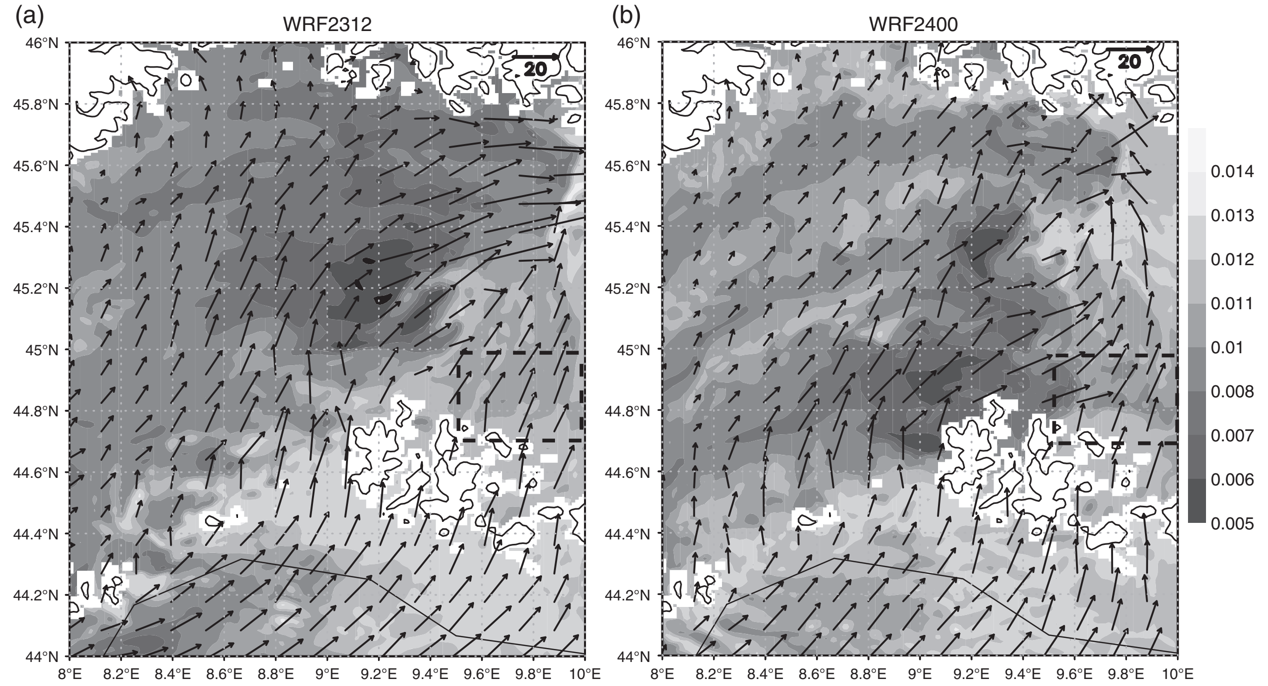

Figure 14. IOP6: as Figures 13(a) and (b), but at 1300 UTC on 24 September 2012.

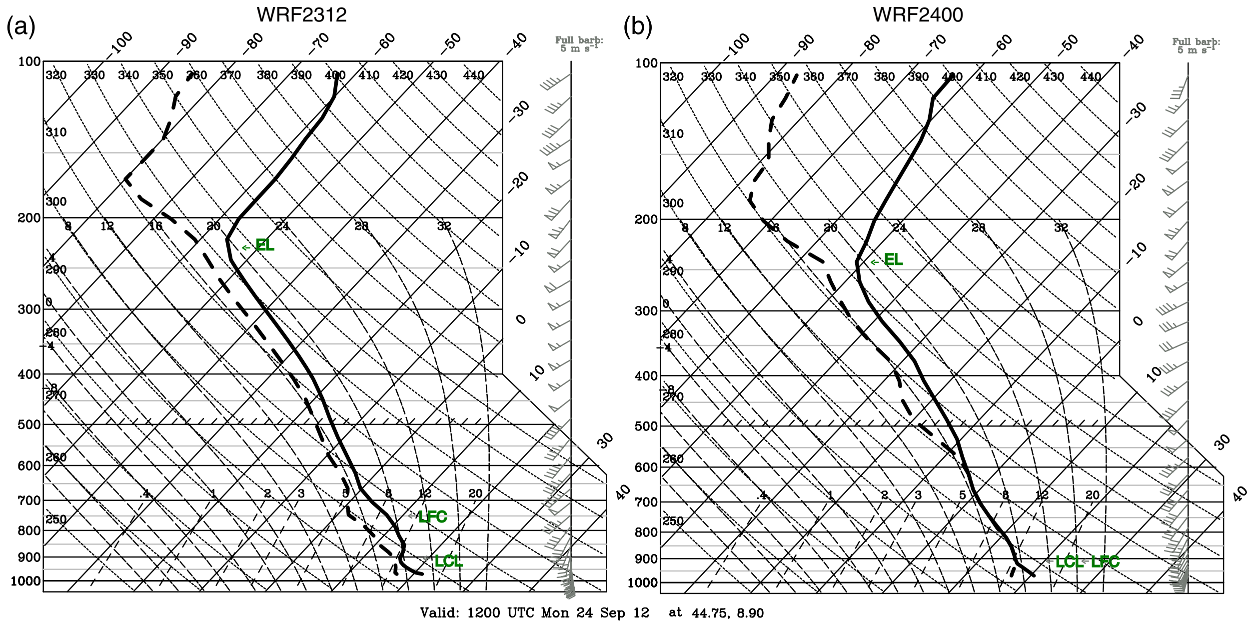

Figure 15. IOP6: dew point temperature (bold dashed black line), temperature (bold solid black line) and horizontal wind profiles on skew-T diagrams at 44.75°N, 8.99°E (sub-Apennines area; indicated by 'R' on Figures 13(a) and (b)) as simulated on the finest horizontal grid (1 km) by (a) WRF2312 and (b) WRF2400 at 1200 UTC on 24 September 2012. Lifting Condensation Level (LCL; at 903 hPa, 911 hPa), Level of Free Convection (LFC; 752 hPa, 911 hPa) and Equilibrium Level (EL; 231 hPa, 245 hPa) are indicated. [Colour figure can be viewed at wileyonlinelibrary.com].

Figure 8(a)), suggesting that some suppression mechanism is already acting in that area. In contrast, the squall-line simulated by WRF2400 (Figure 8(c)) is correctly north–south oriented with approximately correct 50 dBZ cells embedded along its entire extent. Moreover, as the convection over the Gulf of Genoa is part of the squall-line (Figure 8(a)), its correct triggering and evolution also play a role in the correct simulation of the environmental conditions upstream of the Apennines. WRF2312 (Figure 8(b)) misses the off-shore convection while WRF2400 (Figure 8(c)) is somewhat better, showing cells aligned with the frontal squall-line.

By the time of the observations at 1400 UTC, WRF2312 (Figure 8(e)) has very little convection across the Po Valley; both clouds and rain formation are mostly confined to areas where the flow is forced upward by the orography. In contrast, WRF2400 (Figure 8(f)) continues to maintain convective cells north of the Apennines, although the line-like structure is beginning to break apart.

A comparison of the model with the rain-gauge data (Figures 9(a), (d) and (g)) confirms the radar analysis: the observations show the frontal rain crossing northern Italy from west to east, with ORP and HPE over the Alps and Apennines and weaker precipitation across the Po Valley. The WRF2312 and WRF2400 simulations both show rain associated with the squall-line by 1400 UTC (Figures 9(b), (c), (e) and (f)); however casual inspection shows that WRF2400 produces a more realistic rain field than WRF2312 in terms of both rain amounts and pattern of squall-line axis orientation. By 1500 UTC (Figure 9(h)), it is clear that WRF2312 incorrectly suppresses convective activity across the Po Valley, while the rain gauges were still observing rain between 5 and 15 mm h^{-1}; furthermore, WRF2312 overestimates the rain over the pre-Alps and in the northeastern area. In contrast, WRF2400 (Figure 9(i)) maintains rain cells comparable with those observed, even showing rain extinction in the area north of the Apennines near 11°E.

In summary, the extensive number of sensitivity tests we performed using one-way-interactive grid nesting showed only slight differences with respect to the incorrect suppression of convection in the Po Valley in IOP6. Only when interactive nests were used did the simulations begin to allow the model to produce Po Valley convection analogous to that observed. Moreover the simulation with an initial condition closer to the event time produced the best comparison with observations. This sensitivity of Po Valley convection in IOP6 to two-way feedbacks and initial conditions stands in contrast to the forecasts of Po Valley convection in IOP13.

The results of this section indicate that the basic forecast problem is the incorrect suppression of convection on the north side of the Apennines, which happens to be the lee side given the generally southsouthwesterly winds (Figure 5(d)). The occurrence of lee-side subsidence strongly depends on the upstream wind strength and static stability, which may be characterized by the Froude number. The difference in Fr between IOP6 (larger $Fr \rightarrow$ less blocked) and IOP13 (smaller $Fr \rightarrow$ more blocked) was already noted above with respect to flow past the Maritime Alps, which in turn influences conditions downstream over the Gulf of Genoa. These considerations lead us to hypothesize that there is also less-pronounced flow blocking by the Apennines in IOP6 than in IOP13, suggesting an orographic flow modification which is at the threshold between a 'flow-over' and a 'flow-around' configuration in IOP6; this makes for a sensitive forecast of convection downstream. More specifically we will show evidence that the overly strong subsidence on the lee (north) side of the Apennines inhibits frontal convection in WRF2312.

5. Further analysis of WRF simulations of IOP6

The most important differences between WRF2312 and WRF2400 are found in the lower levels (below 850 hPa). In particular, WRF2312 produces stronger winds than WRF2400 over the Gulf of Genoa (i.e. downstream of the Maritime Alps and upstream of the Apennines) as well as a lower static stability close to the coastline. This difference in winds and static stability does not affect the simulated frontal convection until the front passes through the area that connects the Maritime Alps to the Apennines, where the orography is lower (around 430 m asl; Figure 1(a)); ahead of this area, i.e. ahead of the front at 1200 UTC, the stronger winds and weaker static stability bring strong subsidence on the lee (north) side of the Apennines (at around 9°E).

Figure 10 displays the horizontal wind vectors at 200 m above the surface and the potential temperature at 500 m for the two simulations at 1200 and 1300 UTC. Focusing on the winds near the coast in the Gulf of Genoa (in the box), Figures 10(a) and (b) indicate stronger meridional winds in WRF2312 than in WRF2400 at 1200 UTC; these stronger winds dry and warm the air on the lee (north) side of the Apennines ahead the front and produce conditions less favourable to convection in WRF2312 than in WRF2400. As a consequence, the squall-line convection is suppressed in WRF2312 at 1300 UTC relative to WRF2400 (Figures 10(c) and (d)).

We will present further analysis of IOP6 below, but it is convenient at this juncture to present a comparison of IOP6 (Figure 10) with our simulation of IOP13 which was much less sensitive to modelling assumptions and start time. As noted in Table 1, the larger-scale forcing acting in IOP13 is known to produce convection-favourable conditions in the Po Valley. Figure 11 shows the IOP13 simulation (WRF1400, initialized 14 October 2012 at 0000 UTC) in the same format as used in Figure 10 for IOP6. In this case, the eastward passage of the deep upper-level trough produced a classic cyclogenesis (Buzzi and Tibaldi, 1978; Trigo *et al.*, 2002; Buzzi, 2010) in the Gulf of Genoa (Figure 2(b)), which WRF correctly represents; the convergence of the associated southwesterly flow component over the Gulf of Genoa with the southeasterly barrier flow on the north side of the Apennines, triggers convective cells that move over the Po Valley during the earlier period (Figure 11(a)). In the later period, the eastward movement of the lee cyclone produces a southeasterly barrier wind in the Po Valley bringing warm moist air interacting with the northerly flow of colder air flowing over the Alps on the west end of the Po Valley and further convection ensues, even far upstream of the steep terrain of Alps (Figure 11(b)). Similar conditions were documented for IOP8 of MAP (Bousquet and Smull, 2003; Rotunno and Ferretti, 2003); in particular the detailed analysis of observed data by Bousquet and Smull (2003) concludes that one of the impacts of a high degree of blocking upstream of the Alps is to induce a local modulation of low-level convergence associated with cold fronts passing over the Gulf of Genoa, with a consequent release of convective instability across the Po Valley.

A key feature is that the flow on the upwind side of the Apennines is weaker in IOP13 than in IOP6, indicating that it is more blocked and less prone to produce downslope warming on the north side of the Apennines (in the Po Valley) which we will analyze below for IOP6.

The vertical cross-sections in Figure 12 show the Froude number *Fr* as simulated by WRF for IOP6 and IOP13. The cross-sections are representative of the flow ahead of the front for the two cases and show the greater tendency for blocked-flow conditions upstream the Apennines for IOP13 compared with either WRF forecast of IOP6. Profiles extracted at 44°N (Figure 12(d)) well highlight differences among the three simulations. This difference between IOP13 and IOP6 is also confirmed by the ECMWF analyses for the two cases, whose profiles of *Fr* at 44°N (not shown) indicate values between 0.5 and 1 up to 900 hPa and 1–1.5 above for IOP13, whereas for IOP6 $Fr \simeq 1.5$–4 below 900 hPa and 1.5–5 above.

Further evidence for the suppression of frontal convection due to subsidence in IOP6 is supplied in Figure 13 which shows a comparison between the WRF2312 and WRF2400 fields of water vapour mixing ratio at 1200 UTC at 900 hPa (Figures 13(a) and (b)) and vertical cross-sections ahead of the front at 9°E (Figures 13(c) and (d)). The cross-sections in Figures 13(c) and (d) (the black-dashed boxes) show the subsidence drying occurring in WRF2312 on the lee (north) side of the Apennines; this drying is reflected in the horizontal plots (Figures 13(a) and (b)) along 9°E between 44.8 and 45°N (the black-dashed boxes). The comparison between WRF2312 and WRF2400 at 1300 UTC in Figure 14 indicates, in the area highlighted by the black-dashed boxes, that subsidence warming competes with the frontal uplift associated with the cold front and/or convection-produced cold outflows. Apparently WRF2400 (Figure 14(b)) maintains an equilibrium among these factors such that the squall-line survives even when the pre-frontal southwesterly flow impinges on the highest part of the Apennine chain. We speculate that this delicate balance is the reason why only a two-way nested grid with updated ICs was able to produce something similar to the observations in this case.

The skew-*T* plots (Figure 15) taken at 1200 UTC ahead of the front (44.75°N, 8.9°E; 'R' in Figures 13(a) and (b)) for the two simulations indicate that, in addition to the difference in the convective available potential energy (CAPE), there is a marked difference in convective inhibition (CI) – 69 J kg^{-1} (Figure 15(a)) versus 19 J kg^{-1} (Figure 15(b) – which translates to a 160 hPa higher level of free convection (LFC) for WRF2312. In the following hours (not shown), even though differences in CAPE are reduced, WRF2312 constantly shows larger CI than WRF2400, with differences in the range of 30–50 J kg^{-1}.

In summary, these experiments suggest that the sensitivity of the meridional winds across and ahead of the front is a key factor for the predictability of the squall-line convection in IOP6. These winds are part of an orographic flow modification on the scale of the Alps and suggest that the predictability of convection in the Po Valley is limited by the predictability of the orographic flow modification which, in turn, may be limited when the upstream criterion for flow blocking is near the threshold between 'flow-over' and 'flow-around' regimes. These results are consistent with Barrett *et al.* (2014), in which a similar decrease in predictability occurred with an overly high Froude number in cases of orographic rainfall in the Lake District of England.

6. Conclusions

During the first special observation period (SOP1; 5 September–5 November 2012) of the HyMeX project, the western Mediterranean basin was monitored to document heavy and/or orographic precipitation and flash-flood events. In several of the intensive observation periods (IOPs) declared for northern Italy, convection was observed across the Po Valley, but there were several cases in which most of the models available during the SOP1 did a poor job in forecasting it.

As examples of good and poor forecasts we analyze here, respectively, IOP13 (15 October 2012) and IOP6 (24 September 2012). Both events were characterized by eastward-moving, upper-level troughs (deeper for IOP13 than for IOP6), with associated cold fronts and southwesterly flows advecting moist, warm and unstable air across northern Italy. IOP13 was characterized by blocked airflow upstream of the western Alps while IOP6 was characterized by a less pronounced degree of blocking. Both events were characterized by frontal convection across the Po Valley which was correctly forecasted for IOP13 by most of the models available during SOP1, but not for IOP6. Indeed, in IOP6, convection was suppressed by most of the models a few hours after the front passed the western Alps, contrary to what both radars and rain-gauges observed on that day.

The WRF model was used here to investigate the reasons for the failure to forecast convection in the Po Valley in IOP6. A series of different numerical experiments carried out in a one-way-nested configuration (as in the forecast models) were all affected by the incorrect suppression of convection (Table 2). We found that a two-way-nested configuration was necessary, but not sufficient, to produce a realistic representation of the convective squall-line in IOP6, confirming the need for a feedback mechanism in the case of weak large-scale forcing; furthermore only the forecast initialized closer in time to the event was successful. Comparison of the successful simulation (WRF2400) with the unsuccessful one (WRF2312) provides insight into the nature of the forecast sensitivity in IOP6. Since there was no such problem in forecasting Po Valley convection in IOP13, we formed the hypothesis that the greater degree of flow blocking in this case allows for a good frontal-convection forecast in the Po Valley. In particular the weaker flow splitting around the Maritime Alps in IOP6 (compared to IOP13) indicates that the flow was at the threshold between 'flow-over' and 'flow-around' and hence makes for a sensitive forecast for downstream developments (i.e. in the Po Valley).

This sensitivity is illustrated by the comparison between the unsuccessful WRF2312 and the successful WRF2400. The most important differences between the two simulations were found below 850 hPa in the wind and static stability over the Gulf of Genoa. Stronger cross-Apennine (southerly) winds in WRF2312 than in WRF2400 caused subsidence warming and drying of the air ahead the front on the lee side of the Apennines (i.e in the Po Valley) and, in addition, impeded the rear-to-front (across-slope) flow needed to sustain the front and/or frontal-convection cold outflows. These experiments illustrate that orographically induced subsidence on the lee (north) side of the Apennines competes with frontal and/or cold-outflow uplift needed to generate convection. The delicate equilibrium among these factors appears to be crucial for the squall-line survival. We are unaware of any studies reaching similar conclusions for the Po Valley. More generally, the present results are consistent with the findings of Barrett *et al.* (2014), in which a correlation was found between flow blocking and the predictability of lee-side convection over the Lake District of England.

In summary, the orographic flow modification on the scale of the Alps influences the predictability of convection in the Po Valley in cases of weak blocking configurations by the Alpine barrier, such as occurred in IOP6. Our finding, that two-way nesting was necessary to have a least one solution capable of allowing the squall-line convection to persist, points to the importance of feedbacks between convective-scale motions and orographic flow.

Acknowledgements

This work represents a contribution to the HyMeX programme. The authors acknowledge: Météo-France and the HyMeX program for supplying the data, sponsored by grants MISTRALS/HyMeX and ANR-11-BS56-0005 IODA-MED project; the National Center for Atmospheric Research (NCAR) and the Center of Excellence for the integration of remote-sensing TEchniques and numerical Modeling for the Prediction of Severe weather (CETEMPS) for financial and computing resources; NCAR for WRF-ARW source code; the Computational Information Systems Laboratory at the National Center for Atmospheric Research for 3D imagery produced by VAPOR (http://www.vapor.ucar.edu); and the Italian Civil Protection department for rain-gauge data.

References

Asencio N, Stein J, Chong M, Gheusi F. 2003. Analysis and simulation of local and regional conditions for the rainfall over the Lago Maggiore target area during MAP IOP 2b. *Q. J. R. Meteorol. Soc.* **129**: 565–586.

Barrett A, Gray S, Kirshbaum D, Nigel R, Schultz D, Fairman JG. 2014. Synoptic versus orographic control on stationary convective banding. *Q. J. R. Meteorol. Soc.* **141**: 1101–1113.

Borga M, Boscolo P, Zanon F, Sangati M. 2007. Hydro-meteorological analysis of the 29 August 2003 flash flood in the Eastern Italian Alps. *J. Hydrometeorol.* **8**: 1049–1067.

Bougeault P, Binder P, Buzzi A, Dirks R, Houze R, Kuettner J, Smith RB, Steinacker R, Volkert H. 2001. The MAP Special Observing Period. *Bull. Am. Meteorol. Soc.* **82**: 433–462.

Bousquet O, Smull BF. 2003. Observations and impacts of upstream blocking during a widespread orographic precipitation event. *Q. J. R. Meteorol. Soc.* **129**: 391–409.

Bousquet O, Smull B. 2006. Observed mass transports accompanying upstream orographic blocking during MAP IOP8. *Q. J. R. Meteorol. Soc.* **132**: 2393–2413.

Buzzi A. 2010. 'Synoptic-scale variability in the Mediterranean'. In Seminar on Predictability in the European and Atlantic Regions, 6–9 September 2010. ECMWF: Reading, UK.

Buzzi A, Alberoni PP. 1992. Analysis and numerical modelling of a frontal passage associated with thunderstorm development over the Po Valley and the Adriatic Sea. *Meteorol. Atmos. Phys.* **48**: 205–224.

Buzzi A, Foschini L. 2000. Mesoscale meteorological features associated with heavy precipitation in the southern Alpine region. *Meteorol. Atmos. Phys.* **72**: 131–146.

Buzzi A, Tartaglione N, Malguzzi P. 1998. Numerical simulations of the 1994 Piedmont flood: Role of orography and moist processes. *Mon. Weather Rev.* **126**: 2369–2383.

Buzzi A, Tibaldi S. 1978. Cyclogenesis in the lee of the Alps: A case study. *Q. J. R. Meteorol. Soc.* **104**: 271–287.

Cacciamani C, Battaglia F, Patruno P, Pomi L, Selvini A, Tibaldi S. 1995. A climatological study of thunderstorm activity in the Po Valley. *Theor. Appl. Climatol.* **50**: 185–203.

Chou MD, Suarez MJ. 1999. 'A solar radiation parameterization for atmospheric studies', NASA Technical Memorandum 104606. **15**. NASA, United States.

Davolio S, Ferretti R, Baldini L, Casaioli M, Cimini D, Ferrario ME, Gentile S, Loglisci N, Maiello I, Manzato A, Mariani S, Marsigli C, Marzano FS, Miglietta MM, Montani A, Panegrossi G, Pasi F, Pichelli E, Pucillo A, Zinzi A. 2015. The role of the Italian scientific community in the first HyMeX SOP: An outstanding multidisciplinary experience. *Meteorol. Z.* **24**: 261–267. https://doi.org/10.1127/metz/2015/0624.

Davolio S, Volont A, Manzato A, Pucillo A, Cicogna A, Ferrario ME. 2016. Mechanisms producing different precipitation patterns over northeastern Italy: Insights from HyMeX-SOP1 and previous events. *Q. J. R. Meteorol. Soc.* **142**: 188–205. https://doi:10.1002/qj.2731.

Drobinski P, Ducrocq V, Alpert P, Anagnostou E, Beranger K, Borga M, Braud I, Chanzy A, Davolio S, Delrieu G, Estournel C, Filali Boubrahmi N, Font J, Grubisic V, Gualdi S, Homar V, Ivancan-Picek B, Kottmeier C, Kotroni V, Lagouvardos K, Lionello P, Llasat MC, Ludwig W, Lutoff C, Mariotti A, Richard E, Romero R, Rotunno R, Roussot O, Ruin I, Somot S, Taupier-Letage I, Tintore J, Uijlenhoet R, Wernli H. 2014. HyMeX, a 10-year multidisciplinary program on the Mediterranean water cycle. *Bull. Am. Meteorol. Soc.* **95**: 1063–1082. https://doi.org/10.1175/BAMS-D-12-00242.1.

Dudhia J. 1995. Reply. *Mon. Weather Rev.* **123**: 2571–2575.

Ducrocq V, Braud I, Davolio S, Ferretti R, Flamant C, Jansa A, Kalthoff N, Richard E, Taupier-Letage I, Ayral PA, Belamari S, Berne A, Borga M, Boudevillain B, Bock O, Boichard JL, Bouin MN, Bousquet O, Bouvier C, Chiggiato J, Cimini D, Corsmeier U, Coppola L, Cocquerez P, Defer E, Drobinski P, Dufournet Y, Fourrie N, Gourley JJ, Labatut L, Lambert D, Le Coz J, Marzano FS, Molinie G, Montani A, Nord G, Nuret M, Ramage K, Rison B, Roussot O, Said F, Schwarzenboeck A, Testor P, Van Baelen J, Vincendon B, Aran M, Tamayo J. 2014. HyMeX-SOP1, the field campaign dedicated to heavy precipitation and flash flooding in the northwestern Mediterranean. *Bull. Am. Meteorol. Soc.* **95**: 1083–1100. https://doi.org/10.1175/BAMS-D-12-00244.1.

Durran RD, Klemp JB. 1983. A compressible model for the simulation of moist mountain waves. *Mon. Weather Rev.* **111**: 2341–2361.

Ferretti R, Low-Nam S, Rotunno R. 2000. Numerical simulations of the 1994 Piedmont flood of 4-6 November. *Tellus* **52A**: 162–180.

Ferretti R, Pichelli E, Gentile S, Maiello I, Cimini D, Davolio S, Miglietta MM, Panegrossi G, Baldini L, Pasi F, Marzano FS, Zinzi A, Mariani S, Casaioli M, Bartolini G, Loglisci N, Montani A, Marsigli C, Manzato A, Pucillo A, Ferrario ME, Colaiuda V, Rotunno R. 2014. Overview of the first HyMeX special observation period over Italy: Observations and model results. *Hydrol. Earth Syst. Sci.* **18**: 1953–1977. https://doi:10.5194/hess-18-1953-2014.

Gheusi F, Stein J. 2003. Small-scale rainfall mechanisms for an idealized convective southerly flow over the Alps. *Q. J. R. Meteorol. Soc.* **129**: 1819–1839.

Grell GA, Dévényi D. 2002. A generalized approach to parameterizing convection combining ensemble and data assimilation techniques. *Geophys. Res. Lett.* **29**: 1693. https://doi.org/10.1029/2002GL015311.

Medina S, Houze RA. 2003. Air motions and precipitation growth in Alpine storms. *Q. J. R. Meteorol. Soc.* **129**: 345–371.

Miglietta MM, Manzato A, Rotunno R. 2016. Characteristics and predictability of a supercell during HyMeX SOP1. *Q. J. R. Meteorol. Soc.* **142**: 2839–2853. https://doi:10.1002/qj.2872.

Mlawer EJ, Taubman SJ, Brown PD, Iacono MJ, Clough SA. 1997. Radiative transfer for inhomogeneous atmospheres: RRTM, a validated correlated-k model for the longwave. *J. Geophys. Res.* **102**: 16663–16682. https://doi.org/10.1029/97JD00237.

Morgan GM. 1973. A general description of the hail problem in the Po Valley of northern Italy. *J. Appl. Meteorol.* **12**: 338–353.

Nakanishi M, Niino H. 2006. An improved Mellor–Yamada level 3 model: Its numerical stability and application to a regional prediction of advecting fog. *Boundary-Layer Meteorol.* **119**: 397–407.

Niu G-Y, Yang Z-L, Mitchell KE, Chen F, Ek MB, Barlage M, Longuevergne L, Kumar A, Manning K, Niyogi D, Rosero E, Tewari M, Xia Y. 2011. The community Noah land surface model with multiparameterization options (Noah-MP): 1. Model description and evaluation with local scale measurements. *J. Geophys. Res.* **116**: D12109. https://doi.org/10.1029/2010JD015139.

Panziera L, James C, Germann U. 2015. Mesoscale organization and structure of orographic precipitation producing flash floods in the Lago Maggiore region. *Q. J. R. Meteorol. Soc.* **141**: 224–248.

Pichelli E, Ferretti R, Cacciani M, Siani AM, Ciardini V, Di Iorio T. 2014. The role of urban boundary layer investigated with high-resolution models and ground-based observations in Rome area: A step towards understanding parameterization potentialities. *Atmos. Meas. Tech.* **7**: 315–332. https://doi:10.5194/amt-7-315-2014.

Reeves HD, Lin YL. 2006. Effect of stable layer formation over the Po Valley on the development of convection during MAP IOP-8. *J. Atmos. Sci.* **63**: 2567–2584.

Rotunno R, Ferretti R. 2001. Mechanisms of intense Alpine rainfall. *J. Atmos. Sci.* **58**: 1732–1749.

Rotunno R, Ferretti R. 2003. Orographic effects on rainfall in MAP cases IOP2b and IOP8. *Q. J. R. Meteorol. Soc.* **129**: 373–390.

Rotunno R, Houze RA. 2007. Lessons on orographic precipitation from the Mesoscale Alpine Programme. *Q. J. R. Meteorol. Soc.* **133**: 811–830.

Schneidereit M, Schär C. 2000. Idealised numerical experiments of alpine flow regimes and south side precipitation events. *Meteorol. Atmos. Phys.* **72**: 233–250.

Skamarock WC, Klemp JB, Dudhia J, Gill DO, Barker DM, Duda MG, Huang XY, Wang W, Powers JG. 2008. 'A description of the advanced research WRF version 3', Technical Note NCAR/TN-475+STR. NCAR: Boulder, CO.

Thompson G, Field PR, Rasmussen RM, Hall WD. 2008. Explicit forecasts of winter precipitation using an improved bulk microphysics scheme. Part II: Implementation of a new snow parameterization. *Mon. Weather Rev.* **136**: 5095–5115.

Trigo IF, Bigg GR, Davies TD. 2002. Climatology of cyclogenesis mechanisms in the Mediterranean. *Mon. Weather Rev.* **130**: 549–569.

